DOI: 10.1002/chem.200601174

Hydrogencyanamide-Bridged One-Dimensional Polymers Built on Mn^{III}–Schiff Base Fragments: Synthesis, Structure, and Magnetism

Mei Yuan, Fei Zhao, Wen Zhang, Feng Pan, Zhe-Ming Wang, and Song Gao*[a]

Abstract: The ability of $NCNH^-$ to construct transition metal coordination polymers and to transmit magnetic coupling was investigated. By introduction of various tetradentate Schiff base ligands (L) and different solvents (S), nine $NCNH^-$-bridged manganese(III) coordination complexes were obtained. Their structures can be divided into three types: I) NCNH-bridged chains built on mononuclear $[Mn^{III}(L)]$ units, $[Mn^{III}(L)(\mu_{1,3}\text{-}NCNH)]_n$ (L = 5-Brsalen (**1**), 5-Clsalen (**2**)); II) NCNH-bridged chains built on dinuclear $[Mn^{III}{}_2(L)_2]$ units, complexes **3**–**8**, $[Mn^{III}{}_2(L)_2(\mu_{1,3}\text{-}NCNH)]ClO_4{\cdot}S$ (L = salen, 5-Fsalen, 5-Clsalen, 5-OCH_3salen; S = CH_3OH or C_2H_5OH); III) NCNH-bridged Mn^{III} dimers linked by hydrogen bonds into a 1D polymer, $\{[Mn^{III}(3\text{-}OCH_3salen)(H_2O)]_2(\mu_{1,3}\text{-}NCNH)\}ClO_4{\cdot}0.5H_2O$ (**9**, salen = *N*,*N*′-bis(salicylidene)-1,2-diaminoethane). In these complexes, the $N{\equiv}C{-}NH^-$ resonance structure dominates the bonding mode of the $NCNH^-$ ligand adopting the $\mu_{1,3}$-bridging mode. Magnetic characterization shows that the asymmetric $NCNH^-$ bridge transmits antiferromagnetic interaction between Mn^{III} ions and often favors the weak ferromagnetism caused by spin canting in these one-dimensional chains. However, these complexes exhibit different magnetic behaviors at low temperatures.

Keywords: chain structures · magnetic properties · manganese · N ligands · N,O ligands

Introduction

The design and synthesis of transition-metal coordination polymers bridged by small conjugated ligands such as cyano, azido, oxalato, and nitrido are currently under intense investigation in view of their structural diversity and in the context of molecule-based magnets.[1] As a potential nitrogen-based ligand, cyanamide ($NCNH_2$) and its anions ($NCNH^-$ and NCN^{2-}) have been used to prepare a number of alkali metal,[2] alkaline-earth metal,[3] and rare-earth metal[4] salts by different synthetic routes, but their transition metal coordination chemistry and ability to mediate magnetic coupling remain largely unexplored. MnNCN, the first and only carbodiimide of a magnetic transition-metal, was reported by Dronskowski et al. in 2005.[5] Moreover, most structurally characterized transition-metal cyanamide complexes[6–7] have molecular cluster structures, to our knowledge, and only three zero-dimensional $NCNH^-$-bridged coordination complexes have been reported so far.[7] Therefore, to construct magnetic coordination polymers bridged by cyanamide is still a great challenge, and is important for expanding the family of molecule-based magnets. Noteworthily, since $NCNH^-$ is isoelectronic with the azide anion, polymers bridged by $NCNH^-$ analogous to the well-characterized azide-bridged polymers should exist. On the other hand, dicyanamide (dca, $N(CN)^{2-}$) has been widely used as a functional ligand to synthesize coordination polymers with interesting magnetic properties, as well as various topologies due to its versatile coordination modes.[8] Moreover, among these different coordination modes of bridging dca, the $\mu_{1,3}$-M–N≡C–N–M linkage was found to provide the strongest coupling which often leads to long-range magnetic ordering. This observation further inspired us to explore cyanamide as a bridging ligand to obtain a new series of coordination polymers with interesting magnetic properties. After many attempts, a series of tetradentate Schiff base ligands (Scheme 1) was found not only to stabilize manganese(III) ions with high electron spin and large zero-field splitting, but also to provide an appropriate environment for the coor-

[a] Dr. M. Yuan, F. Zhao, Dr. W. Zhang, F. Pan, Prof. Dr. Z.-M. Wang, Prof. Dr. S. Gao
Beijing National Laboratory for Molecular Sciences
State Key Laboratory of Rare Earth Materials Chemistry and Applications
College of Chemistry and Molecular Engineering, Peking University
Beijing 100871 (P. R. China)
Fax: (+86) 10-6275-1708
E-mail: gaosong@pku.edu.cn

Supporting information for this article is available on the WWW under http://www.chemeurj.org/ or from the author.

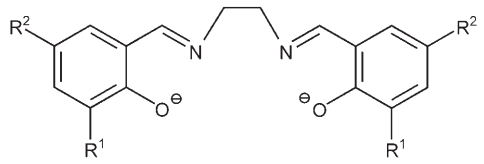

salen^{2-}	$R^1 = R^2 = H$
5-Fsalen^{2-}	$R^1 = H$, $R^2 = F$
5-Clsalen^{2-}	$R^1 = H$, $R^2 = Cl$
5-Brsalen^{2-}	$R^1 = H$, $R^2 = Br$
5-OCH_3salen^{2-}	$R^1 = H$, $R^2 = OCH_3$
3-OCH_3salen^{2-}	$R^1 = OCH_3$, $R^2 = H$

Scheme 1. Schiff base ligands used in this work.

dination of H_2NCN. We previously reported the first hydrogencyanamide-bridged coordination polymer $[Mn^{III}(5\text{-Brsalen})(\mu_{1,3}\text{-NCNH})]_n$ (**1**), which is a mononuclear-Mn^{III}-based one-dimensional chain and shows weak ferromagnetic ordering at low temperature due to spin canting and unusual spin reorientation induced by an applied field.[9]

Here we present the full syntheses and magnetic characterization of eight new NCNH-bridged coordination complexes with a series of tetradentate Schiff base ligands H_2L as auxiliary ligands: $[Mn^{III}(5\text{-Clsalen})(\mu_{1,3}\text{-NCNH})]_n$ (**2**), $[Mn^{III}_2(salen)_2(\mu_{1,3}\text{-NCNH})]ClO_4\cdot CH_3OH$ (**3**), $[Mn^{III}_2(salen)_2(\mu_{1,3}\text{-NCNH})]ClO_4\cdot C_2H_5OH$ (**4**), $[Mn^{III}_2(5\text{-Fsalen})_2(\mu_{1,3}\text{-NCNH})]ClO_4\cdot CH_3OH$ (**5**), $[Mn^{III}_2(5\text{-Fsalen})_2(\mu_{1,3}\text{-NCNH})]ClO_4\cdot C_2H_5OH$ (**6**), $[Mn^{III}_2(5\text{-Clsalen})_2(\mu_{1,3}\text{-NCNH})]ClO_4\cdot CH_3OH$ (**7**), $[Mn^{III}_2(5\text{-}OCH_3\text{salen})_2(\mu_{1,3}\text{-NCNH})]ClO_4\cdot C_2H_5OH$ (**8**), $\{[Mn^{III}(3\text{-}OCH_3\text{salen})(H_2O)]_2(\mu_{1,3}\text{-NCNH})\}ClO_4\cdot 0.5H_2O$ (**9**) (salen = *N*,*N*′-bis(salicylidene)-1,2-diaminoethane). Their crystal structures can be divided into three types: I) NCNH-bridged chains built on mononuclear $[Mn^{III}(L)]$ units (**1** and **2**); II) NCNH-bridged chains built on dinuclear $[Mn^{III}_2(L)_2]$ units (**3**–**8**); III) NCNH-bridged Mn^{III} dimers linked by hydrogen bonds into a 1D polymer (**9**). Magnetic characterization shows that the asymmetric $NCNH^-$ bridge transmits antiferromagnetic interaction between Mn^{III} ions and often favors the weak ferromagnetism caused by spin canting in these one-dimensional chains. However, these complexes exhibit different magnetic behaviors at low temperatures.

Abstract in Chinese:

本文首次对 $NCNH^-$作为桥连配体来构筑过渡金属配位聚合物以及传递磁耦合作用的能力进行了研究。通过采用不同的四齿西佛碱（L）作为辅助配体以及溶剂（S）的变化，我们成功得到九个 $NCNH^-$桥连的锰（III）配位聚合物。它们的结构可以分成三类：I）基于单核的$[Mn^{III}(L)]$ 单元由 NCNH 桥连形成的链，$[Mn^{III}(L)(\mu_{1,3}\text{-NCNH})]_n$ [L = 5-Brsalen (**1**)、5-Clsalen (**2**)]；II） 基于双核的$[Mn^{III}_2(L)_2]$单元由NCNH 桥连形成的链**3**—**8**，$Mn^{III}_2(L)_2(\mu_{1,3}\text{-NCNH})](ClO_4)\cdot S$ [L = salen、5-Fsalen、5-Clsalen、5-OCH_3salen；S = CH_3OH 或 C_2H_5OH]；III）基于 NCNH 桥连的 Mn^{III} 双核化合物进一步由多重氢键连接形成的一维聚合物，$\{[Mn^{III}(3\text{-}OCH_3\text{salen})(H_2O)]_2(\mu_{1,3}\text{-NCNH})\}(ClO_4)\cdot 0.5H_2O$ **9** (salen = *N*,*N*′-bis(salicylidene)-1,2-diaminoethane)。 在这些化合物中，$NCNH^-$ 配体均采取$\mu_{1,3}$ 桥连方式，以共振形式 N≡C–NH^-为主。磁性测定表明在这些一维的 Mn^{III} 配合物中，不对称短桥 $NCNH^-$传递的主要是反铁磁相互作用，并且非常易于产生自旋倾斜导致的弱铁磁性。然而，它们在低温区却表现出各自不同的磁学行为，将在正文中详述。

Results and Discussion

Synthesis: H_2NCN is a weak acid and needs to be neutralized by a certain base to enhance its ability to coordinate to transition metals. On the other hand, H_2NCN is vulnerable to degeneration in strongly basic or acid environments and loses its coordination ability.[10] Also, in an alkaline environment, most transition metals are liable to form precipitates. These disadvantages made it difficult to obtain single crystals in our syntheses. Complexes **1**–**9** were all prepared by the method of solvent evaporation. The choice of solvent (methanol or ethanol) and base (NaOH or triethylamine) depended on the Schiff base ligands. For example, with $H_2$5-Clsalen, methanol as solvent and NaOH as neutralizing base were preferred, while H_2-5OCH_3salen was suited to ethanol and triethylamine. In comparison, H_2salen and $H_2$5-Fsalen were both insensitive to solvents and bases, and therefore two pairs of similar complexes **3**/**4** and **5**/**6** were obtained only with different solvent molecules. During the preparation of complexes **1**–**8**, it was found that under similar reaction conditions, Mn^{III}-dimer-based complexes were more easily formed than mononuclear Mn^{III} complexes. The use of $Mn(CH_3COO)_2\cdot 4H_2O$ can favor the formation of mononuclear Mn^{III} complexes, and $Mn(ClO_4)_2\cdot 6H_2O$ Mn^{III}-dimer-based complexes, for example, the syntheses of complexes **2** and **7**. We also tried to use this strategy to obtain mononuclear Mn^{III} complexes with H_2salen, $H_2$5-OCH_3salen, or $H_2$5-Fsalen ligands, but sufficiently large single crystals for X-ray characterization could not be obtained, only polycrystalline powders in low yield. Complex **9** is an NCNH-bridged Mn^{III} dimer with multiple hydrogen bonds that differs from the polymeric structures of **1**–**8** due to the different position of the OCH_3 substituent.

FTIR spectra: The IR spectra of complexes **1**–**9** all exhibit strong absorption at 2100–2150 cm^{-1}, assignable to the asymmetric stretching vibration of the NCNH moiety. These values are much lower than those observed for the neutral H_2NCN ligand (2220–2260 cm^{-1}).[7a,11] Also, the characteristic absorptions of CH and NH groups were also detected at about 2900–3350 cm^{-1}. In Mn^{III}-dimer-based complexes **3**–**8**, the strong absorption at about 1090 cm^{-1} and the weak bands at 3500–3600 cm^{-1} are attributed to the characteristic vibrations of ClO_4^- and solvent molecules, respectively.

Crystal structures of 1 and 2 (structure type I): Crystallographic data for **1** and **2** are listed in Table 1, and selected bond lengths and angles in Table 2. Single-crystal X-ray analysis revealed that **2** has a similar structure to that of **1**, which was reported previously,[9] except for the Schiff base ligand 5-Clsalen instead of 5-Brsalen. As shown in Figure 1, complex **2** also features an NCNH-bridged mononuclear-Mn^{III}-based chain. There is only one crystallographically independent manganese atom in a distorted octahedral geometry, which is coordinated by the N_2O_2 donor atoms from one 5-Clsalen ligand in the equatorial mode and two N donor atoms from two $NCNH^-$ ions in the axial positions. Each $NCNH^-$ ligand functions as a *trans*-$\mu_{1,3}$ bridge to link monomeric $[Mn^{III}(5\text{-Clsalen})]^+$ units into a one-dimensional zigzag chain (Figure 1b), comparable to $\mu_{1,3}$-N_3 bridged chains.[12] In the equatorial plane, Mn1, O1, O2, N1, and N2 are nearly coplanar. The Mn1–O1, Mn1–O2, Mn1–N1, and Mn1–N2 bond lengths of 1.879(1), 1.885(1), 1.996(2), and 1.975(2) Å, respectively, are close to those in other Mn^{III} salen complexes.[12b] As expected, the axial Mn1–N3 and Mn1–N4A bond lengths (2.245(2) and 2.376(2) Å, respectively) are elongated due to Jahn–Teller distortion at the high-spin d^4 metal center,[12] which also indicates unsymmetric coordination of the NCNH bridge. For comparison, in the previously reported dinuclear structure of $[Cu_2(C_9H_{21}N_3)_2(\mu\text{-NCNH})_2]]ClO_4{\cdot}2H_2O$ ($C_9H_{21}N_3$ = N,N′,N″-trimethyl-1,4,7-triazacyclononane), which also has an end-to-end NCNH bridge, the NCNH bridges are approximately symmetrical, with Cu–N distances ranging from 1.962(5) to 2.017(6) Å.[7b]

In complex **2**, the C17–N3H and C17–N4 bond lengths of 1.303(3) and 1.175(3) Å, as well as the N4-C17-N3H angle of 174.4(2)°, emphasize the importance of resonance structure $N{\equiv}C{-}NH^-$ (a) over resonance structure $N^-{=}C{=}NH$ (b)

Table 1. Crystallographic data for **1**–**9**.

	1	**2**	**3**	**4**	**5**
formula	$C_{17}H_{13}Br_2MnN_4O_2$	$C_{17}H_{13}Cl_2MnN_4O_2$	$C_{34}H_{33}ClMn_2N_6O_9$	$C_{35}H_{35}ClMn_2N_6O_9$	$C_{34}H_{29}ClF_4Mn_2N_6O_9$
FW	520.07	431.15	814.99	829.02	886.96
crystal system	monoclinic	monoclinic	triclinic	triclinic	triclinic
space group	$P2_1/c$	$P2_1/c$	$P\bar{1}$	$P\bar{1}$	$P\bar{1}$
a [Å]	13.3699(4)	13.242(3)	11.378(2)	11.323(2)	11.467(2)
b [Å]	11.7277(4)	11.758(2)	12.278(3)	12.298(3)	12.162(2)
c [Å]	11.5495(3)	11.508(2)	13.582(3)	13.463(3)	13.927(3)
α [°]	90	90	110.46(3)	83.36(3)	78.48(3)
β [°]	105.978(2)	108.00(3)	98.19(3)	74.31(3)	77.98(3)
γ [°]	90	90	93.57(3)	87.01(3)	86.01(3)
V [Å^3]	1740.98(9)	1704.0(6)	1746.7(6)	1792.4(6)	1860.7(6)
Z	4	4	2	2	2
ρ_{calcd} [g cm^{-3}]	1.984	1.681	1.550	1.536	1.583
μ [mm^{-1}]	5.369	1.109	0.863	0.843	0.832
$F(000)$	1016	872	836	852	900
reflections collected	32779	33257	32596	33348	32887
unique reflections	3984	3899	7918	8197	8472
GoF	0.979	0.987	0.893	0.968	0.898
R_1[a]	0.0326	0.0342	0.0478	0.0416	0.0488
wR_2[b]	0.0670	0.0715	0.0945	0.1092	0.1044

	6	**7**	**8**	**9**
formula	$C_{35}H_{31}ClF_4Mn_2N_6O_9$	$C_{34}H_{29}Cl_5Mn_2N_6O_9$	$C_{39}H_{43}ClMn_2N_6O_{13}$	$C_{37}H_{42}ClMn_2N_6O_{14.5}$
FW	900.99	952.76	949.12	948.10
crystal system	triclinic	triclinic	triclinic	triclinic
space group	$P\bar{1}$	$P\bar{1}$	$P\bar{1}$	$P\bar{1}$
a [Å]	11.428(2)	11.488(2)	11.393(2)	12.083(2)
b [Å]	12.224(2)	12.250(3)	12.107(2)	13.718(3)
c [Å]	14.095(3)	14.796(3)	15.801(3)	14.707(3)
α [°]	85.83(3)	88.16(3)	80.39(3)	62.77(3)
β [°]	73.45(3)	70.75(3)	79.97(3)	83.21(3)
γ [°]	86.31(3)	85.56(3)	86.91(3)	88.55(3)
V [Å^3]	1880.5(6)	1960.1(7)	2115.3(7)	2151.3(7)
Z	2	2	2	2
ρ_{calcd} [g cm^{-3}]	1.591	1.614	1.490	1.464
μ [mm^{-1}]	0.825	1.046	0.731	0.721
$F(000)$	916	964	980	978
reflections collected	37310	34548	39872	36324
unique reflections	8588	8938	9630	9766
GoF	0.927	1.016	0.923	0.910
R_1[a]	0.0419	0.0477	0.0521	0.0567
wR_2[b]	0.0816	0.1068	0.1201	0.1324

[a] $R_1 = \Sigma||F_o|-|F_c||/\Sigma|F_o|$. [b] $wR_2 = [\Sigma w(F_o^2-F_c^2)^2/\Sigma w(F_o^2)^2]^{1/2}$.

Table 2. Selected bond lengths [Å] and angles [°] of **1**–**9**.

		1 (#1: $x, -y+1/2, z+1/2$; #2: $x, -y+1/2, z-1/2$)			
Mn1−O2	1.8801(18)	O2-Mn1-N1	175.69(9)	O2-Mn1-N4#1	91.59(9)
Mn1−O1	1.8812(19)	O1-Mn1-N1	92.15(9)	O1-Mn1-N4#1	94.94(9)
Mn1−N1	1.976(2)	O2-Mn1-N2	93.20(9)	N1-Mn1-N4#1	85.67(9)
Mn1−N2	1.991(2)	O1-Mn1-N2	175.21(9)	N2-Mn1-N4#1	83.63(9)
Mn1−N3	2.245(2)	N1-Mn1-N2	83.20(9)	N3-Mn1-N4#1	168.50(9)
Mn1−N4#1	2.407(3)	O2-Mn1-N3	94.52(9)	C17-N3-Mn1	125.9(2)
N3−C17	1.294(4)	O1-Mn1-N3	94.64(9)	C17-N4-Mn1#2	138.3(2)
N4−C17	1.171(4)	N1-Mn1-N3	87.63(9)	N4-C17-N3	174.3(3)
O2-Mn1−O1	91.40(8)	N2-Mn1-N3	86.31(9)		
		2 (#1 $x, -y+1/2, z+1/2$; #2: $x, -y+1/2, z-1/2$)			
Mn1−O1	1.8785(14)	O1-Mn1-N2	176.08(7)	O1-Mn1-N4#1	92.31(7)
Mn1−O2	1.8848(14)	O2-Mn1-N2	92.14(7)	O2-Mn1-N4#1	94.75(7)
Mn1−N2	1.9751(17)	O1-Mn1-N1	92.83(7)	N2-Mn1-N4#1	86.32(7)
Mn1−N1	1.9956(17)	O2-Mn1-N1	175.37(7)	N1-Mn1-N4#1	83.86(7)
Mn1−N3	2.2454(17)	N2-Mn1-N1	83.38(7)	N3-Mn1-N4#1	169.15(6)
Mn1−N4#1	2.3761(18)	O1-Mn1-N3	93.87(7)	C17-N3-Mn1	125.59(15)
N3−C17	1.303(3)	O2-Mn1-N3	93.97(7)	C17-N4-Mn1#2	138.25(17)
N4−C17	1.175(3)	N2-Mn1-N3	86.93(7)	N4-C17-N3	174.4(2)
		O1-Mn1-O2	91.63(6)	N1-Mn1-N3	86.93(7)
		3 (#1: $-x, -y+1, -z+1$; #2: $-x+1, -y+2, -z+1$)			
Mn1−O2	1.863(2)	O1-Mn1-N2	165.68(10)	O3-Mn2-N3	92.00(11)
Mn1−O1	1.904(2)	O2-Mn1-N1	172.17(11)	O4-Mn2-N3	169.40(11)
Mn1−N2	1.970(3)	O1-Mn1-N1	89.34(10)	N4-Mn2-N3	82.26(12)
Mn1−N1	1.983(2)	N2-Mn1-N1	82.34(11)	O3-Mn2-N6	98.88(11)
Mn1−N5	2.165(3)	O2-Mn1-N5	95.37(10)	O4-Mn2-N6	96.75(10)
Mn1−O1#1	2.526(2)	O1-Mn1-N5	98.99(11)	N4-Mn2-N6	91.50(11)
Mn2−O3	1.869(2)	N2-Mn1-N5	92.79(12)	N3-Mn2-N6	90.66(11)
Mn2−O4	1.903(2)	N1-Mn1-N5	90.77(11)	O3-Mn2-O4#2	86.37(9)
Mn2−N4	1.967(3)	O2-Mn1-O1#1	89.23(9)	O4-Mn2-O4#2	82.25(9)
Mn2−N3	1.979(3)	O1-Mn1-O1#1	81.16(9)	N4-Mn2-O4#2	83.33(10)
Mn2−N6	2.195(3)	N2-Mn1-O1#1	86.45(10)	N3-Mn2-O4#2	89.67(10)
Mn2−O4#2	2.513(2)	N1-Mn1-O1#1	84.61(9)	N6-Mn2-O4#2	174.72(9)
N5−C33	1.267(4)	N5-Mn1-O1#1	175.38(8)	C33-N5-Mn1	125.7(2)
N6−C33	1.202(4)	O3-Mn2-O4	94.32(9)	C33-N6-Mn2	121.7(2)
O2-Mn1−O1	94.50(9)	O3-Mn2-N4	168.21(11)	N6-C33-N5	175.1(3)
O2-Mn1−N2	92.47(10)	O4-Mn2-N4	89.95(10)		
		4 (#1: $-x+1, -y, -z$)			
Mn2−O3	1.8732(17)	O3-Mn2-N3	92.15(8)	O2-Mn1-N1	171.65(8)
Mn2−O4	1.8983(17)	O4-Mn2-N3	166.16(7)	O1-Mn1-N1	89.56(8)
Mn2−N3	1.980(2)	O3-Mn2-N4	169.02(7)	N2-Mn1-N1	82.04(9)
Mn2−N4	1.983(2)	O4-Mn2-N4	89.45(8)	O2-Mn1-N5	96.49(8)
Mn2−N6	2.166(2)	N3-Mn2-N4	81.49(8)	N1-Mn1-N5	89.58(8)
Mn1−O2	1.8704(17)	O3-Mn2-N6	97.29(8)	O2-Mn1-O1#1	90.97(7)
Mn1−O1	1.9132(16)	O4-Mn2-N6	96.14(8)	O1-Mn1-O1#1	79.11(7)
Mn1−N2	1.980(2)	N3-Mn2-N6	94.65(8)	N2-Mn1-O1#1	89.30(7)
Mn1−N1	1.985(2)	N4-Mn2-N6	92.17(9)	N1-Mn1-O1#1	83.41(7)
Mn1−N5	2.160(2)	O2-Mn1-O1	95.47(7)	N5-Mn1-O1#1	171.56(7)
Mn1−O1#1	2.4768(17)	O2-Mn1-N2	91.74(8)	C33-N5-Mn1	127.01(16)
N5−C33	1.261(3)	O1-Mn1-N2	166.42(8)	C33-N6-Mn2	128.07(19)
N6−C33	1.182(3)	O1-Mn1-N5	96.19(8)	N6-C33-N5	175.9(3)
		O3-Mn2-O4	95.05(7)	N2-Mn1-N5	94.41(9)
		5 (#1: $-x+1, -y, -z+1$)			
Mn1−O1	1.859(2)	O1-Mn1-N1	92.09(12)	O4-Mn2-O3	94.58(10)
Mn1−O2	1.910(2)	O2-Mn1-N1	166.99(10)	O4-Mn2-N3	168.88(11)
Mn1−N1	1.975(3)	O1-Mn1-N2	172.66(11)	O3-Mn2-N3	89.43(11)
Mn1−N2	1.988(3)	O2-Mn1-N2	88.87(11)	O4-Mn2-N4	91.79(11)
Mn1−N5	2.170(3)	N1-Mn1-N2	82.85(13)	O3-Mn2-N4	167.65(11)
Mn1−O2#1	2.484(2)	O1-Mn1-N5	95.69(11)	N3-Mn2-N4	82.46(12)
Mn2−O4	1.870(2)	O2-Mn1-N5	97.88(11)	O4-Mn2-N6	98.41(11)
Mn2−O3	1.896(2)	N1-Mn1-N5	92.13(12)	O3-Mn2-N6	96.92(11)
Mn2−N3	1.980(3)	N2-Mn1-N5	89.83(11)	N3-Mn2-N6	91.38(12)
Mn2−N4	1.981(3)	O1-Mn1-O2#1	87.96(9)	N4-Mn2-N6	92.59(12)
Mn2−N6	2.177(3)	O2-Mn1-O2#1	81.19(9)	C33-N5-Mn1	126.6(3)
N5−C33	1.254(4)	N1-Mn1-O2#1	88.29(10)	C33-N6-Mn2	122.1(3)
N6−C33	1.202(4)	N2-Mn1-O2#1	86.58(10)	N6-C33-N5	176.0(4)
		O1-Mn1−O2	95.14(10)	N5-Mn1-O2#1	176.31(10)

Table 2. (Continued)

		6 (#1: $-x+1, -y+1, -z$)			
Mn1−O1	1.8641(17)	O1-Mn1-N2	172.62(9)	O4-Mn2-O3	94.69(7)
Mn1−O2	1.9064(17)	O2-Mn1-N2	89.46(8)	O4-Mn2-N3	169.28(8)
Mn1−N2	1.981(2)	O1-Mn1-N1	92.04(8)	O3-Mn2-N3	89.66(8)
Mn1−N1	1.984(2)	O2-Mn1-N1	165.85(8)	O4-Mn2-N4	91.81(8)
Mn1−N5	2.161(2)	N2-Mn1-N1	82.59(9)	O3-Mn2-N4	166.17(8)
Mn1−O2#1	2.4871(19)	O1-Mn1-N5	96.26(8)	N3-Mn2-N4	81.95(9)
Mn2−O4	1.8676(18)	O2-Mn1-N5	98.16(9)	O4-Mn2-N6	98.21(8)
Mn2−O3	1.8963(16)	N2-Mn1-N5	89.13(9)	O3-Mn2-N6	96.45(8)
Mn2−N3	1.978(2)	N1-Mn1-N5	93.42(9)	N3-Mn2-N6	91.02(9)
Mn2−N4	1.979(2)	O1-Mn1-O2#1	90.01(7)	N4-Mn2-N6	94.69(9)
Mn2−N6	2.168(2)	O2-Mn1-O2#1	80.43(8)	C33-N5-Mn1	126.99(18)
N5−C33	1.276(3)	N2-Mn1-O2#1	84.70(8)	C33-N6-Mn2	125.97(19)
N6−C33	1.183(3)	N1-Mn1-O2#1	87.17(8)	N6-C33-N5	176.5(3)
		O1-Mn1−O2	94.73(7)	N5-Mn1-O2#1	173.67(7)
		7 (#1: $-x+1, -y+1, -z+1$)			
Mn1−O1	1.859(2)	O1-Mn1-N1	92.60(11)	O4-Mn2-O3	94.82(10)
Mn1−O2	1.908(2)	O2-Mn1-N1	167.44(10)	O4-Mn2-N3	168.28(10)
Mn1−N1	1.972(3)	O1-Mn1-N2	173.03(11)	O3-Mn2-N3	89.48(11)
Mn1−N2	1.975(3)	O2-Mn1-N2	89.69(11)	O4-Mn2-N4	91.60(11)
Mn1-N5	2.178(3)	N1-Mn1-N2	82.57(12)	O3-Mn2-N4	166.67(11)
Mn1−O2#1	2.446(2)	O1-Mn1-N5	95.74(11)	N3-Mn2-N4	82.09(12)
Mn2−O4	1.872(2)	O2-Mn1-N5	98.16(10)	O4-Mn2-N6	97.82(11)
Mn2−O3	1.902(2)	N1-Mn1-N5	91.68(11)	O3-Mn2-N6	96.56(11)
Mn2−N3	1.974(3)	N2-Mn1-N5	89.45(11)	N3-Mn2-N6	92.50(11)
Mn2−N4	1.984(3)	O1-Mn1-O2#1	87.84(9)	N4-Mn2-N6	94.12(11)
Mn2−N6	2.175(3)	O2-Mn1-O2#1	80.81(9)	C33-N5-Mn1	125.43(24)
C33−N6	1.192(4)	N1-Mn1-O2#1	88.89(9)	C33-N6-Mn2	121.14(24)
C33−N5	1.249(5)	N2-Mn1-O2#1	87.04(10)	N6-C33-N5	175.6(4)
		O1-Mn1−O2	94.16(10)	N5-Mn1-O2#1	176.35(10)
		8 (#1: $-x, -y+1, -z$)			
Mn1−O2	1.864(2)	O2-Mn1-N2	92.52(13)	O6-Mn2O5	95.42(10)
Mn1−O1	1.905(3)	O1-Mn1-N2	166.22(11)	O6-Mn2-N3	91.62(11)
Mn1−N2	1.978(3)	O2-Mn1-N1	172.15(12)	O5-Mn2-N3	166.34(11)
Mn1−N1	1.996(3)	O1-Mn1-N1	89.12(12)	O6-Mn2-N4	169.39(11)
Mn1−N5	2.160(3)	N2-Mn1-N1	81.79(15)	O5-Mn2-N4	89.39(11)
Mn1−O1#1	2.482(3)	O2-Mn1-N5	95.79(11)	N3-Mn2-N4	81.84(12)
Mn2−O6	1.868(2)	O1-Mn1-N5	97.42(12)	O6-Mn2-N6	98.63(12)
Mn2−O5	1.903(2)	N2-Mn1-N5	92.92(13)	O5-Mn2-N6	95.77(12)
Mn2−N3	1.977(3)	N1-Mn1-N5	89.92(12)	N3-Mn2-N6	94.72(12)
Mn2−N4	1.984(3)	O2-Mn1-O1#1	89.39(10)	N4-Mn2-N6	90.27(12)
Mn2−N6	2.165(3)	O1-Mn1-O1#1	80.76(10)	C37-N5-Mn1	127.9(3)
N5−C37	1.282(5)	N2-Mn1-O1#1	88.12(11)	C37-N6-Mn2	126.3(3)
N6−C37	1.176(4)	N1-Mn1-O1#1	85.04(11)	N6-C37-N5	176.5(4)
		O2-Mn1-O1	95.46(11)	N5-Mn1-O1#1	174.66(10)
		9 (#1: $-x+1, -y+1, -z$)			
Mn2−O4	1.878(3)	O3-Mn2-N4	173.47(14)	O2-Mn1-N2	90.79(14)
Mn2−O3	1.886(2)	O4-Mn2-N3	172.35(12)	O1-Mn1-N2	172.23(14)
Mn2−N4	1.964(3)	O3-Mn2-N3	91.89(13)	N1-Mn1-N2	82.48(15)
Mn2−N3	1.972(4)	N4-Mn2-N3	82.88(16)	O2-Mn1-N5	92.92(14)
Mn2−N6	2.194(4)	O4-Mn2-N6	97.39(14)	O1-Mn1-N5	96.30(13)
Mn2−OW2	2.362(3)	O3-Mn2-N6	94.93(13)	N1-Mn1-N5	88.02(15)
Mn1−O2	1.883(3)	N4-Mn2-N6	88.81(15)	N2-Mn1-N5	89.15(14)
Mn1−O1	1.891(3)	N3-Mn2-N6	87.77(15)	O2-Mn1-OW1	89.64(14)
Mn1−N1	1.976(4)	O4-Mn2-OW2	92.95(12)	O1-Mn1-OW1	90.12(13)
Mn1−N2	1.984(3)	O3-Mn2-OW2	90.55(11)	N1-Mn1-OW1	88.68(14)
Mn1−N5	2.211(3)	N4-Mn2-OW2	84.81(13)	N2-Mn1-OW1	84.17(13)
Mn1−OW1	2.325(3)	N3-Mn2-OW2	81.37(14)	N5-Mn1-OW1	172.89(13)
N6−C37	1.267(6)	N6-Mn2-OW2	167.99(13)	C37-N5-Mn1	126.1(3)
C37−N5	1.176(6)	O2-Mn1-O1	94.44(12)	C37-N6-Mn2	128.0(3)
		O4-Mn2-O3	93.28(11)	O2-Mn1-N1	173.20(13)
		N5-C37-N6	175.7(5)	O4-Mn2-N4	91.54(14)
		O1-Mn1-N1	92.15(14)		

in the bonding description of the $NCNH^-$ bridge.[11a–b] The intrachain distance between the two Mn^{III} centers bridged by the $NCNH^-$ ion is about 5.849 Å, which is longer than that in the complex $[Mn(salen)N_3]$.[12b] Similar to that of complex **1**, the nearest interchain Mn···Mn separation is as small as 5.357 Å owing to the rich hydrogen-bonding inter-

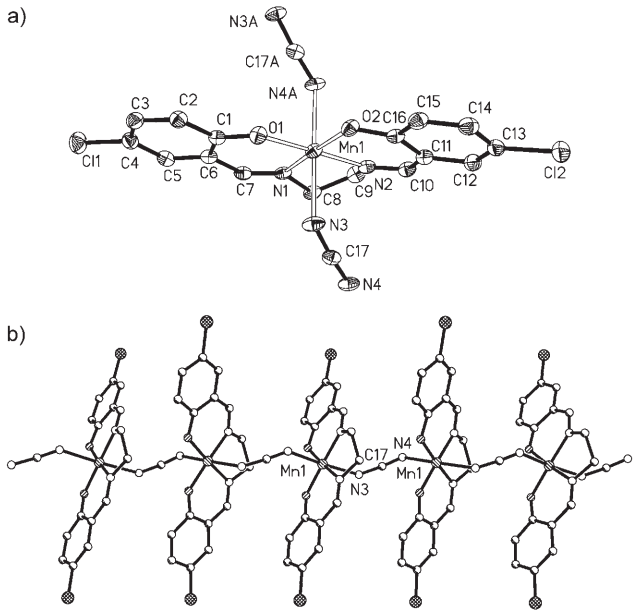

Figure 1. a) ORTEP plot of **2** (30% probability ellipsoids). b) The mononuclear-Mn^{III}-based zigzag chain of **2**.

actions in the packing of **2** (see Figure S1 in the Supporting Information). The hydrogen bond is formed between N3H of the $NCNH^-$ ion and O1 of the 5-Clsalen ligand with an N3···O1 distance of 3.139 Å (Table 3), leading to a two-dimensional supramolecular network. There is little difference between the corresponding bond lengths and angles of complexes **1** and **2** (see Table 2), and hence their magnetic properties are very similar.

Crystal structures of complexes 3–8 (structure type II): Crystallographic data for **3–8** are listed in Table 1, and selected bond lengths and angles in Table 2. The crystal structures of complexes **3–8** all consist of one-dimensional NCNH-bridged Mn^{III}-dimer-based chains (see Figures 2–5), perchlorate counterions, and solvent molecules. The few structural changes brought about by different solvent molecules and/or Schiff base ligands lead to their various magnetic properties (see below). Some pertinent bond lengths and angles for the Mn^{III}-dimer-based chains are listed in Table 4.

*Complexes **3** and **4***: These two complexes are isostructural except for the solvent molecule in the crystal: one methanol molecule for **3** and one ethanol molecule for **4**. As shown in Figure 2a,b, the Mn^{III}-dimer-based chain of **3** or **4** contains two crystallographically independent Mn^{III} atoms in distorted octahedral coordination environments. In the equatorial plane, each Mn center bonds to four donors of a salen ligand. The mean Mn–N and Mn–O bond lengths are 1.975(3), 1.885(2) Å for **3** and 1.983(2), 1.889(2) Å for **4**, respectively, which are close to those in complexes **1** and **2**. In the axial position, each Mn atom is further coordinated to a phenolate oxygen atom (O*) of the neighboring $[Mn^{III}(salen)]^+$ unit to form a dimeric $[Mn^{III}_2(salen)_2]^{2+}$ fragment, which is further linked through $NCNH^-$ ligands into a one-dimensional zigzag Mn^{III}-dimer-based chain comparable to that in **1** and **2** (Figure 2c and Figure S2a in the Supporting Information). A perchlorate ion further balances the charge in the crystal. The Mn–O* bond lengths (2.526(2), 2.513(2) Å for **3** and 2.477(2) Å, 2.587(2) Å for **4**) are much longer than those between the Mn center and intramolecular phenolate oxygen atom. The Mn-O-Mn* angles are 98.84(9), 97.75(9)° for **3** and 100.89(7), 97.49(7)° for **4**. In the chain of **3** or **4**, the intradimer Mn···Mn distances are 3.389 (Mn1···Mn1*), 3.350 Å (Mn2···Mn2*) for **3** and 3.404, 3.402 Å for **4**; the nearest interdimer Mn···Mn distance is 5.521 Å for **3** and 5.558 Å for **4**. The nearest interchain Mn···Mn separation is considerably larger (**3**: 6.699 Å; **4**: 6.699 Å) in comparison with those in **1** and **2**. Interestingly, the Mn1 ion bonds to amido nitrogen donor N5H, while the Mn2 ion is coordinated to cyano nitrogen donor N6 of the same $NCNH^-$ ligand. The corresponding Mn1–N5H and Mn2–N6 lengths of 2.165(3), 2.195(3) Å for **3** and 2.160(2), 2.166(2) Å for **4** are nearly equal, especially for **4**, and are clearly different from those in **1** and **2**. In contrast, the corresponding Mn1-N5H-

Table 3. H-bonds in complexes **1–9**.

	D–H	*d*(D–H) [Å]	*d*(H···A) [Å]	∢(D–H···A) [°]	*d*(D···A) [Å]	A
1	N3–H3A	0.860	2.398	146.68	3.152	O1 [$-x+1, -y+1, -z+1$]
2	N3–H3A	0.860	2.404	143.74	3.139	O1 [$-x+1, -y, -z$]
3	O9–H9	0.820	2.115	159.57	2.898	N6
	N5–H5B	0.860	2.138	146.22	2.892	O9 [$-x+1,-y+1,-z+1$]
4	O9–H9A	0.820	2.448	111.82	2.895.	N6
	N5–H5B	0.860	2.096	169.90	2.946	O9 [$-x+2, -y, -z$]
5	O9–H9	0.820	2.086	170.29	2.897	N6 [$-x+2, -y, -z+1$]
	N5–H5B	0.860	2.095	151.13	2.878	O9
6	O9–H9	0.820	2.579	105.09	2.905	N6
	N5–H5A	0.860	2.077	163.39	2.912	O9 [$-x+2, -y+1, -z$]
7	O9–H9	0.820	2.139	155.36	2.905	N6 [$-x, -y+1, -z+1$]
	N5–H5A	0.860	2.131	149.47	2.904	O9
8	O13–H13A	0.820	2.598	104.32	2.911	N6
	N5–H5A	0.860	2.062	164.30	2.899	O13 [$-x+1, -y+1, -z$]
9	C28–H28	0.930	2.553	130.41	3.234	N5 [$-x, -y+1, -z+1$]
	OW1–HW1A	0.721	2.282	145.44	2.904	O2 [$-x, -y, -z+1$]
	OW1–HW1A	0.721	2.355	146.92	2.985	O6 [$-x, -y, -z+1$]
	OW2–HW2A	0.836	2.145	165.61	2.962	O8 [$-x+1, -y+1, -z+1$]
	OW2–HW2A	0.836	2.384	123.62	2.931	O4 [$-x+1, -y+1, -z+1$]
	OW2–HW2B	0.801	2.155	144.36	2.844	O3 [$-x+1, -y+1, -z+1$]
	OW2–HW2B	0.801	2.308	143.88	2.992	O7 [$-x+1, -y+1, -z+1$]
	OW1–HW1B	0.872	2.202	144.37	2.954	O1 [$-x, -y, -z+1$]
	OW1–HW1B	0.872	2.248	144.23	2.999	O5 [$-x, -y, -z+1$]

Table 4. Pertinent bond lengths [Å] and angles [°] for the NCNH-bridged Mn^{III} complexes **1**–**9**.

	Mn–O*	Mn-O-Mn*	Mn···Mn* (intradimer)	Mn···Mn* (interdimer)	Mn···Mn* (interchain)	Mn···NC (NCNH)	C–N (NCNH)	N-C-N (NCNH)
1	–	–	5.878[a]	–	5.386	138.3(2)	1.294(4)	174.3(3)
						125.9(2)	1.171(4)	
2	–	–	5.849[a]	–	5.357	138.25(17)	1.303(3)	174.4(2)
						125.59(15)	1.175(3)	
3	2.526(2)	98.84(9)	3.389	5.521	6.699	125.7(2)	1.267(4)	175.1(3)
	2.513(2)	97.75(9)	3.350			121.7(2)	1.202(4)	
4	2.477(2)	100.89(7)	3.404	5.558	6.699	128.07(9)	1.261(3)	175.9(3)
	2.587(2)	97.49(7)	3.402			127.01(6)	1.182(3)	
5	2.484(2)	98.81(9)	3.372	5.503	6.692	126.6(3)	1.254(4)	176.0(4)
	2.568(2)	96.97(9)	3.357			122.1(3)	1.202(4)	
6	2.591(2)	99.56(8)	3.376	5.537	6.677	126.99(18)	1.276(3)	176.5(3)
	2.487(2)	97.48(7)	3.404			125.97(19)	1.183(3)	
7	2.446(2)	99.19(9)	3.431	5.480	6.758	125.43(4)	1.249(5)	175.6(4)
	2.641(2)	96.73(9)	3.334			121.14(4)	1.192(4)	
8	2.482(3)	99.24(9)	3.413	5.547	6.590	127.9(3)	1.282(5)	176.5(4)
	2.578(3)	98.11(3)	3.363			126.3(3)	1.176(4)	
9	–	–	5.742	4.827	7.093	128.0(3)	1.267(6)	175.7(5)
				4.888		126.1(3)	1.176(6)	

[a] Intrachain.

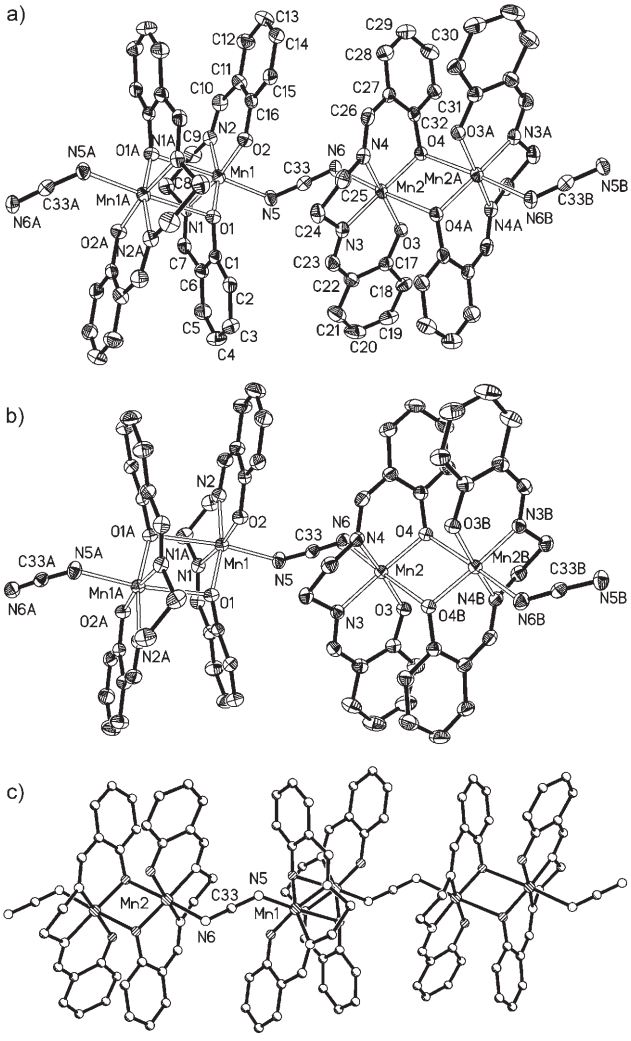

Figure 2. a) ORTEP plot of **3** (30% probability ellipsoids). b) ORTEP plot of **4** (30% probability ellipsoids). c) The Mn^{III}-dimer-based chain of **3**.

C33 and Mn2-N6-C33 angles of **3** and **4** are different: 125.7(2), 121.7(2)° for **3** and 127.0(2), 128.2(2)° for **4**, respectively. Therefore, the NCNH ligand in complex **4** acts more like a symmetrical bridge in construction of the one-dimensional Mn^{III}-dimer-based coordination polymer than that in **3**, although the NCNH ligand itself mainly adopts the $N{\equiv}C{-}NH^-$ resonance structure in both **3** and **4** (see below). As expected, elongated bonds in the axial direction were also observed for **3** and **4** because of Jahn–Teller distortion at the Mn^{III} center.

In the $NCNH^-$ bridge, the C33–N5H and C33–N6 bond lengths and N5H-C33-N6 bond angle are 1.267(4), 1.202(4) Å, 175.1(3)° for **3** and 1.261(3), 1.182(3) Å, 175.9(3)° for **4**, respectively, which again indicate that resonance structure $N{\equiv}C{-}NH^-$ (a) dominates the bonding mode of the NCNH ligand in **3** and **4**. A comparison of the bond parameters between **2** and **3**, respectively, follows: NH–C: 1.294(4), 1.267(4) Å; C≡N: 1.171(4), 1.202(4) Å; NH–C≡N: 174.3(3), 175.3(4)°. These differences may suggest a greater contribution of resonance form b in **3** than in **2**, since NH–C is shorter, C≡N is longer, and the NH–C=N angle is closer to 180° for the NCNH ligand in **3**.

In the space packing of **3** and **4** (see Figure S2b,c in the Supporting Information), the hydrogen bonds are stronger than those in mononuclear-Mn^{III}-based chains **1** and **2** because of the introduction of solvent molecules, and they lead to a two-dimensional supramolecular network containing perchlorate anions in the cavities. The double hydrogen bonds are formed between N5H or N6 of the $NCNH^-$ ion and O9H of the solvent molecule. The N5···O9 and N6···O9 distances of **3** are very close to those of **4** (**3**: 2.892, 2.898 Å; **4**: 2.946, 2.895 Å; Table 3), while the corresponding N5–H···O9 and N6···H–O9 angles show a large difference between **3** and **4** (**3**: 146.22, 159.57 Å; **4**: 169.90, 111.82°). These differences may be one of the reasons why the magnetic properties of **3** and **4** are so different.

*Complexes **5** and **6***: These two complexes are another pair of isostructural Mn^{III}-dimer-based chains that only differ in the solvent molecule in the crystal: one methanol molecule for **5** and one ethanol molecule for **6**. As shown in Figure 3 a–c, their structures are very similar to those of **3** and **4**. In the equatorial plane, each Mn center bonds to four donors of one 5-Fsalen ligand. The mean Mn–N and Mn–O bond lengths of 1.981, 1.884 Å for **5** and 1.981, 1.884 Å for **6** are very close to each other. In the dimeric $[Mn^{III}_2(5\text{-Fsalen})_2]^{2+}$ fragment, the Mn–O* bond lengths are 2.484 (2), 2.568 (2) Å for **5** and 2.487(2) Å, 2.591(2) Å for **6**. The

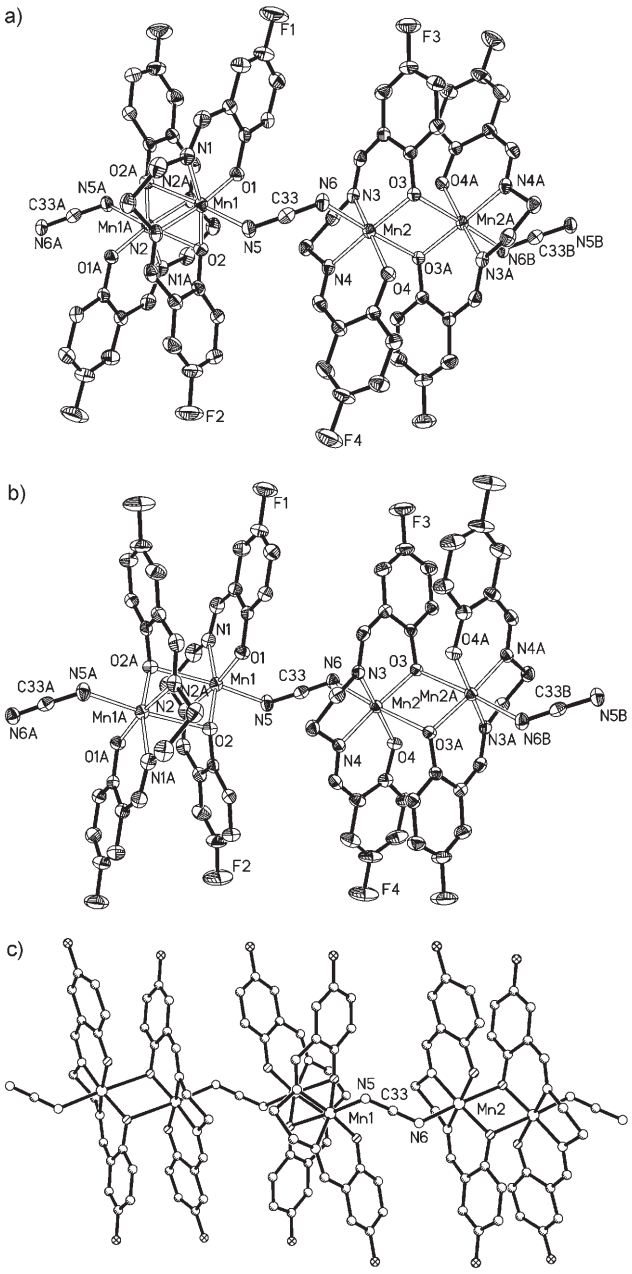

Figure 3. a) ORTEP plot of **5** (30% probability ellipsoids). b) ORTEP plot of **6** (30% probability ellipsoids). c) The Mn^{III}-dimer based chain of **5**.

Mn-O-Mn* angles are 98.81(9), 96.97(9)° for **5** and 99.56(8), 97.48(7)° for **6**. In the chains of complexes **5** and **6** (Figure 3c and Figure S3a in the Supporting Information), the intradimer Mn···Mn distances are 3.357 (Mn1···Mn1*), 3.372 (Mn2···Mn2*) Å for **5** and 3.376, 3.407 Å for **6**; the nearest interdimer Mn···Mn distance is 5.503 Å for **5** and 5.537 Å for **6**, respectively. The nearest interchain Mn···Mn separation is close to those of complexes **3** and **4** (**5**: 6.692 Å; **6**: 6.677 Å). The corresponding Mn1–N5H and Mn2–N6 distances of 2.170(3), 2.177(3) Å for **5** and 2.161(2), 2.168(2) Å for **6**, which are both nearly equal and similar to those in **4**; the corresponding Mn1-N5H-C33 and Mn2-N6-C33 angles of **5** and **6** show a large difference: 126.6(2), 122.1(2)° for **5** and 127.0(2)°, 126.0(2) for **6**, respectively. In contrast, the NCNH ligand in **6** is more like a symmetrical bridge than that in **5**. In the $NCNH^-$ bridge, the C33–N5H and C33–N6 bond lengths (1.254(4), 1.202(4) Å for **5**, and 1.276(3), 1.183(3) Å for **6**), together with the N5H-C33-N6 bond angle (**5**: 176.0(4)°; **6**: 176.5(3)°), again indicate that resonance structure $N{\equiv}C{-}NH^-$ (a) dominates the bonding mode of the NCNH ligand in **5** and **6**. Similar hydrogen bonds to those in **3** and **4** also exist in the crystal packing of **5** and **6** (see Figure S3b,c in the Supporting Information and Table 3). The N5···O9 and N6···O9 distances are 2.878, 2.897 Å and 2.912, 2.905 Å, respectively, while the corresponding N5–H···O9 and N6···H–O9 angles show large differences between **5** and **6** (**5**: 151.13, 170.29°; **6**: 163.39, 105.09°). All the structural data discussed above illustrate the similarities and differences between two pairs of Mn^{III}-dimer-based chains only differing in solvent molecules (**5**/**6** and **3**/**4**).

Complex **7**: In the crystal structure of **7** (Figure 4), the Schiff base ligand is 5-Clsalen, and the solvent molecule is methanol. In the equatorial plane, the mean Mn–N and

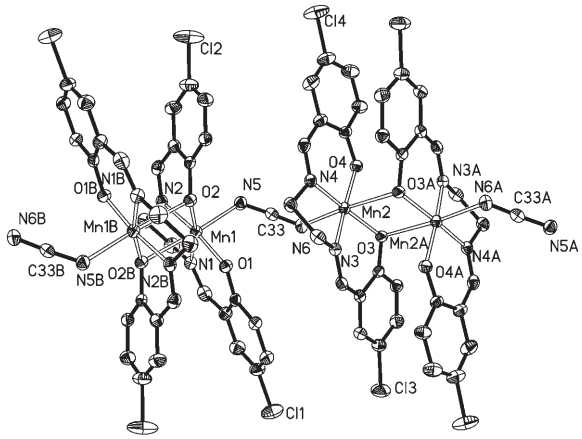

Figure 4. ORTEP plot of **7** (30% probability ellipsoids).

Mn–O bond lengths are 1.976(3) and 1.885(2) Å, respectively. In the axial positions, the Mn–O* distances are 2.446(2) and 2.641(2) Å, and the Mn-O-Mn* angles are 99.19(9) and 96.73(9)°. In the chain of complex **7** (see Figure S4a in the Supporting Information), the intradimer Mn–Mn distances and the nearest interdimer Mn···Mn distance are 3.334, 3.431, and 5.480 Å, respectively. The nearest interchain Mn···Mn separation is 6.758 Å. The Mn1–N5H and Mn2–N6 distances (2.178(3), 2.175(3) Å) are very close to each other and comparable to those in **4**–**6**. However, the Mn1-N5H-C33 and Mn2-N6-C33 angles (125.4(4), 121.1(4)°) have a clear difference, similar to those of complexes **3** and **5**, which also have methanol solvent molecules, but different from those of **4** and **6** with ethanol solvent molecules. In the

$NCNH^-$ bridge, the C33–N5H and C33–N6 bond lengths of 1.249(5) and 1.192(4) Å indicate the dominance of resonance structure $N{\equiv}C{-}NH^-$ (a). Also, in the space packing of complex **7** (see Figure S4b in the Supporting Information) there are hydrogen-bonding interactions between N5H or N6 of the $NCNH^-$ ligand and O9 of the methanol molecule. The N5···O9 and N6···O9 distances are 2.904 and 2.905 Å; the corresponding N5–H···O9 and N6···H–O9 angles are 149.47, 155.36°, respectively, and thus show a relatively small difference similar to those of **3** and **5** with methanol as solvent molecule (Table 3).

*Complex **8***: The crystal structure of **8** is similar to those of **3–7** apart from the Schiff base ligand 5-OCH_3salen (Figure 5) and an ethanol solvent molecule. In the equatorial plane, each Mn ion is coordinated to N_2O_2 donors of one 5-OCH_3salen ligand. The mean Mn–N and Mn–O bond lengths of 1.984(1) and 1.885(2) Å, respectively, are close to those in **1–7**. In the axial direction, the dimeric $[Mn^{III}_2(5\text{-}OCH_3salen)_2]^{2+}$ units connected by phenolate oxygen atoms are further linked into a zigzag chain through $NCNH^-$ bridges (see Figure S5a in the Supporting Information). The Mn–O* distances of 2.482(3) and 2.583(3) Å are comparable to those of **4** and **6**. The Mn-O-Mn* angles are 99.19(9) and 96.73(9)°. In the chain of complex **8**, the intradimer Mn···Mn distances and the nearest interdimer Mn···Mn distance are 3.363, 3.413, and 5.547 Å, respectively, and the nearest interchain Mn···Mn separation is 6.590 Å. The Mn1–N5H and Mn2–N6 bond lengths are 2.160(3) and 2.165(3) Å, and the corresponding Mn1-N5H-C33 and Mn2-N6-C33 angles are 127.9(3) and 126.3(3)°. These values are very similar to those of **4** and **6**, but different from those of **3** and **5**, and this indicates a symmetrical $NCNH^-$ bridge, like in **4** and **6**. In the $NCNH^-$ bridge, the C33–N5H and C33–N6 bond lengths of 1.282(5), 1.176(4) Å also prove the dominance of resonance structure $N{\equiv}C{-}NH^-$ (a). Comparable to **3–7**, hydrogen-bonding interactions exist between N5H or N6 of the $NCNH^-$ ligand and O9 of the ethanol molecule (see Figure S5b in the Supporting Information). The N5···O9 and N6···O9 distances are 2.899 and 2.911 Å, respectively; the corresponding N5–H···O9 and N6···H–O9 angles of 164.30 and 104.32°, respectively, show a relatively large difference similar to complexes **4** and **6** with ethanol as solvent molecules (Table 3).

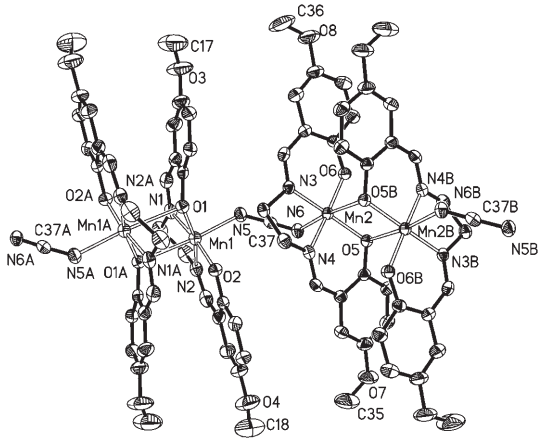

Figure 5. ORTEP plot of **8** (30% probability ellipsoids).

Crystal structure of complex 9 (Structure type III): Crystallographic data for **9** are listed in Table 1, and selected bond lengths and angles in Table 2. The crystal structure of **9** consists of a $NCNH^-$-bridged Mn^{III} dimer, a perchlorate counterion, and half a water molecule. As shown in Figure 6, there are two crystallographically independent Mn^{III} ions. In the equatorial plane, each Mn^{III} center coordinates to O1, N1, N2, and O2 from 3-OCH_3salen^{2-} with mean Mn–N and Mn–O bond lengths of 1.974 and 1.885 Å, respectively. In the apical positions, two Mn^{III} centers are bound through the nitrogen ends of $NCNH^-$ ions with long Mn1–N5 and Mn2–N6 distances of 2.211(3) and 2.194(4) Å and significantly bent Mn1-N5-C37 and Mn2-N6-C37 angles of 126.1(3) and 128.0(3)°, respectively. The opposing coordination site on each Mn^{III} center is taken up by a water molecule (Mn1–OW1 2.325(3), Mn2–OW2 2.362(3) Å). As expected, these distances in the axial position are significantly longer than those associated with the 3-OCH_3salen ligand due to Jahn–Teller distortion at the Mn^{III} center. The distance between two Mn^{III} centers within one dimer of 5.742(2) Å (Mn1···Mn2) is much longer than that in the Mn^{III} dimer fragments linked through phenolate oxygen atoms in **3–8**. Hydrogen bonds exist between the O atom of the coordinated water molecule and that of the intermolecular 3-OCH_3salen ligand with a mean O···O distance of 2.946 Å (see Figure S6 in the Supporting Information). The Mn···Mn distances linked through hydrogen bonds of 4.888 (Mn1···Mn1) and 4.827 Å (Mn2···Mn2) are much shorter than that linked by the NCNH bridge. From this viewpoint, the structure of **9** may also be regarded as a chain constructed of dimeric $[Mn(3\text{-}OCH_3salen)(H_2O)]_2^{2+}$ fragments, like

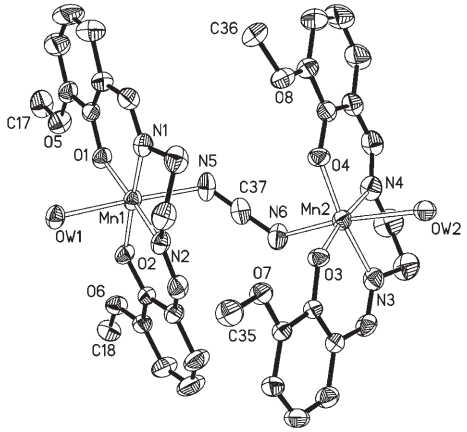

Figure 6. ORTEP plot of **9** (30% probability ellipsoids).

structure type II. The 1D chains are further connected by weak hydrogen-bonding interaction between the N5 atom of the NCNH ligand and the C28 atom of the 3-OCH_3salen ligand of the neighboring chain with a C28···N5 distance of 3.234 Å into a 2D network with perchlorate anions and water solvent molecules alternately embedded in the cavities. The relevant hydrogen-bond lengths and angles are also listed in Table 3.

Magnetic properties: Magnetic measurements were carried out on crystalline samples of complexes **1–9**. According to the obtained data, dominant antiferromagnetic coupling between the Mn^{III} ions in **1–9** can be suggested. However, at low temperature, they show various magnetic behaviors. Detailed discussion of the magnetic properties of **1** can be found elsewhere[9] and will not be presented here.

Complex ***2***: The magnetic properties of **2** are shown in Figure 7. Figure 7a presents the temperature dependence of the magnetic susceptibility from 1.9 to 300 K in a 1 kOe field. On cooling, χ_m increases slowly from 0.01 cm^3mol^{-1} at 300 K to a maximum value of 0.093 cm^3mol^{-1} at about 4.5 K, below which a small decrease indicates the presence of antiferromagnetic (AF) coupling. The data above 100 K obey the Curie–Weiss law with $C=2.92$ $cm^3mol^{-1}K$ and $\theta=-25.2$ K. The Curie constant is close to that of 3.0 $cm^3mol^{-1}K$ expected for one uncoupled spin-only Mn^{III} ion, while the negative θ value confirms dominant AF coupling between Mn^{III} ions. Although this occurs at very low temperatures where anisotropy may be significant, Mn^{III} is expected to be Heisenberg-like in its magnetic properties.[12a] Data fitting similar to that of **1** was used for **2**, and the best fit of the magnetic data above 1.9 K in terms of the Heisenberg one-dimensional chain and the Fisher model[13] with $H=-2JS_{Mn}S_{Mn}$ gives an intrachain coupling of $J=-0.88(5)$ cm^{-1}, an interchain coupling of $zJ'=-1.0(4)$ cm^{-1} ($z=4$), and $g=2.00(4)$ with $R=4.5\times10^{-3}$ ($R=\Sigma[(\chi_mT)_{obsd}-(\chi_mT)_{calcd}]^2/\Sigma(\chi_mT)^2_{obsd}$). Fitting the same set of data using the model given by Weng and modified by Hiller[14] gives the following best-fit parameters: $J=-0.71(3)$ cm^{-1}, $zJ'=-1.9(3)$ cm^{-1} ($z=4$), and $g=2.00$ (fixed) with $R=3.1\times10^{-3}$. These values are clear proof of AF coupling between not only intrachain Mn^{III} ions but also interchain Mn^{III} centers, possibly due to the short interchain Mn···Mn distance in the crystal structure of **2**. This phenomenon was also observed in **1**. The plots of the zero-field cooled (ZFC) and field-cooled (FC) $M(T)$ data (Figure 7b) clearly show two transitions: one is a broad peak attributed to the AF short-range ordered phase at about 9 K (inset); the other is an abrupt increase of the magnetization below about 6.0 K that indicates weak ferromagnetism due to spin canting at low field. To investigate the magnetic behavior at low temperature, the χ_m versus T curves were measured in different fields in the range of 1–40 kOe (Figure 7c). The weak ferromagnetism is greatly influenced by increasing applied field: 1) the characteristic spin-canting peak becomes weaker and weaker until it disappears completely at 20 kOe; 2) the point at which the weak ferromagnetic phase occurs moves to lower temperature with increasing applied field. On the other hand, similar to complex **1**, the shape of the characteristic peak of AF ordering at about 8.0–9.0 K in **2** shows an obvious change at about 40 kOe, which indicates another magnetic transition, possibly from a spin-canted AF phase to another AF state. This unusual field-induced spin reorientation was further confirmed by plots of M versus H measured at different temperatures (Figure 7d). We found that the curves of M versus H below about 6.0 K all exhibit an inflection point as the applied field increases. The critical field of about 37 kOe was determined from the dM/dH versus H curve. Moreover, the magnetization only reaches a value of about $0.73N\beta$ mol^{-1} at 50 kOe, clearly far from the theoretical saturation value of $4N\beta$ mol^{-1} (for Mn^{III}: $g=2$, $S=2$). The ac magnetic susceptibility data (see Figure S7a in the Supporting Information) also reveal the appearance of magnetic ordering in **2**. A critical temperature of $T_C=5.1$ K was

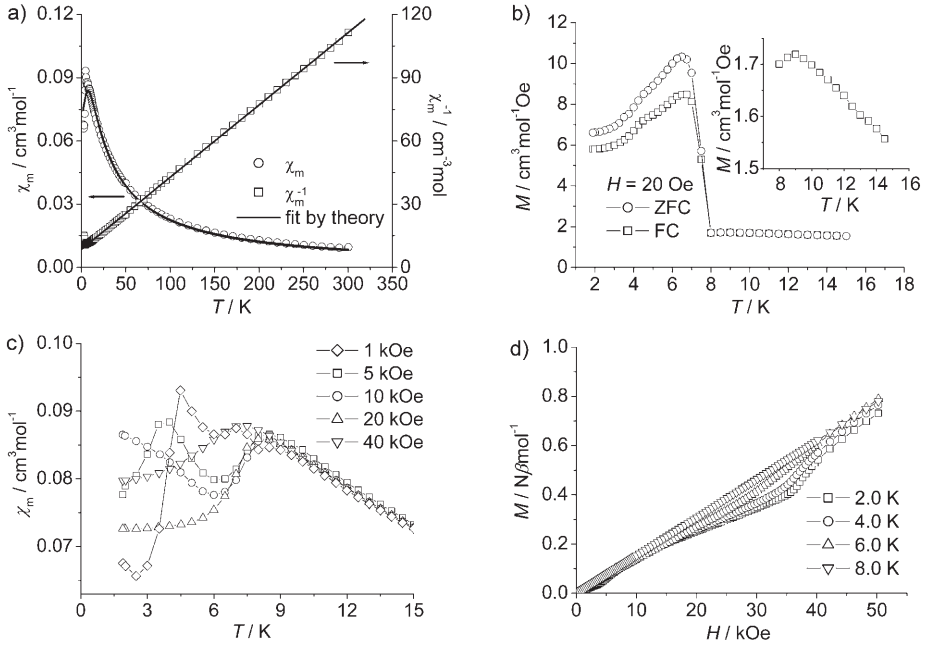

Figure 7. a) χ_m and χ_m^{-1} versus T plots in an applied field of 1 kOe with a theoretical fit for **2**. b) Plots of FC and ZFC magnetization for **2**. The inset is part of the enlarged FC magnetization plot of **2**. c) χ_m versus T plots at different fields. d) Field dependence of magnetization at different temperatures.

determined from the peak of the χ_m' versus T plot, whereas another peak at about 8.5 K in the χ_m' versus T curve gave a critical temperature of AF ordering of $T_N = 8.5$ K. Furthermore, a hysteresis loop was detected in the ordered phase at 1.80 K (see Figure S7b in the Supporting Information), characteristic of a weak ferromagnet, but its shape is a little strange in comparison with that of complex **1**, presented only in the short-field range of 2–6 kOe. This also reflects the complicated field-dependent behavior of magnetization of **2**.

*Complexes **3**–**8***: Magnetic susceptibility of the Mn^{III}-dimer-based chains **3**–**8** was measured at a field of 1 kOe in the range of 2–300 K. The $\chi_m T$ versus T plots of **3**–**8** are shown in Figure 8. The $\chi_m T$ values for these complexes at room temperature are in the range of 5.61–5.84 $cm^3 mol^{-1} K$ (per Mn^{III}_2 unit), in good agreement with 6.0 $cm^3 mol^{-1} K$ for two noninteracting high-spin Mn^{III} ions ($S = 2$). On cooling, the $\chi_m T$ value decreases gradually down to a minimum, which reveals an overall antiferromagnetic coupling between Mn^{III} ions in complexes **3**–**8**. However, with further cooling, the $\chi_m T$ value for complexes **3** and **5**–**7** exhibits an abrupt increase to a maximum and then decreases again, possibly due to the effect of zero-field splitting (ZFS) arising from the Mn^{III} ion and/or a field-saturation effect, whereas the $\chi_m T$ values for **4** and **8** do not show any anomaly. The sharp increase of $\chi_m T$ in the low temperature range for **3** and **5**–**7** may be attributed to weak ferromagnetism due to spin canting. The magnetic susceptibility above 100 K for all six complexes can be fit to the Curie–Weiss law [$\chi_m = C/(T-\theta)$] and give the following parameters: $C = 6.22$ $cm^3 mol^{-1} K$, $\theta = -26.7$ K for **3**; $C = 6.28$ $cm^3 mol^{-1} K$, $\theta = -35.2$ K for **4**; $C = 6.26$ $cm^3 mol^{-1} K$, $\theta = -24.1$ K for **5**; $C = 6.19$ $cm^3 mol^{-1} K$, $\theta = -26.1$ K for **6**; $C = 6.31$ $cm^3 mol^{-1} K$, $\theta = -34.7$ K for **7**; and $C = 6.33$ $cm^3 mol^{-1} K$, $\theta = -31.4$ K for **8**. The Curie constants C of 6.19–6.33 $cm^3 mol^{-1} K$ for **3**–**8** also agree well with two independent high-spin Mn^{III} ions (per Mn^{III}_2 unit). The negative Weiss constants θ for **3**–**8** further confirm antiferromagnetic coupling in **3**–**8**. The various magnetic behaviors of complexes **3**–**8** in the low-temperature region are discussed in detail below.

The χ_m versus T curves of **3** measured at different fields (50–1000 Oe) are shown in Figure 9a. A sharp maximum around 3 K in low fields (50–600 Oe) which disappears at high field (>1 kOe) indicates AF ordering at low field and a metamagnetic transition at high field, probably from antiferromagnet to weak ferromagnet. The T_N value can be estimated to be about 3.2 K from the maximum of $d(\chi_m T)/dT$. To confirm the metamagnetic behavior in **3**, the field dependence of magnetization at 1.9 K (Figure 9b) was measured. It shows a sigmoidal shape, characteristic of metamagnetic behavior. Below 1 kOe, the magnetization increases slightly with increasing field; subsequently, it rises more steeply, but only reaches about $1.22 N\beta\,mol^{-1}$ at 50 kOe, far from the expected saturation value of $8.0 N\beta\,mol^{-1}$ (for two Mn^{III} ions: $g = 2$, $S = 2$). The small magnetization at high field further proves the state of weak ferromagnetism arising from spin canting in **3**. The "double-S" shape of the hysteresis loop at 1.9 K further confirms the occurrence of metamagnetic behavior. The critical field is approximately 1 kOe at 1.9 K. The temperature dependence of the ac magnetic susceptibilities (Figure 9c) confirms the antiferromagnetic ordering

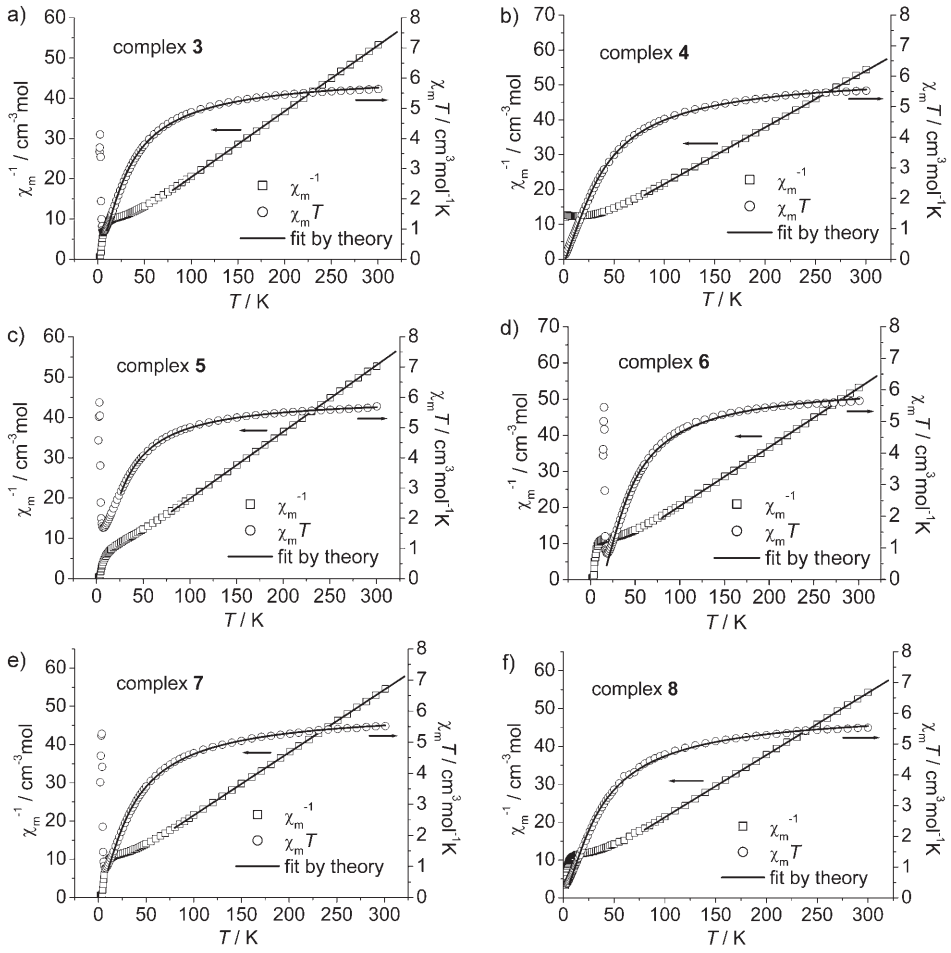

Figure 8. Plots of temperature dependence of $\chi_m T$ with theoretical fits for **3**–**8** at 1 kOe field and 2–300 K.

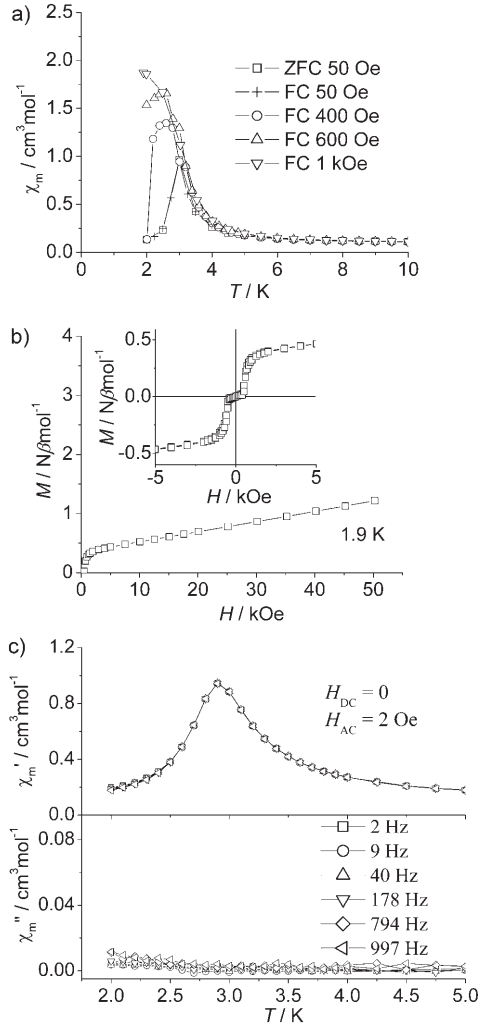

Figure 9. a) χ_m versus T plots at different fields for **3**. b) M versus H plot at 1.9 K for **3**. The inset is the hysteresis loop for **3**. c) Real χ_m' and imaginary χ_m'' ac magnetic susceptibility as a function of temperature at different frequencies for **3**.

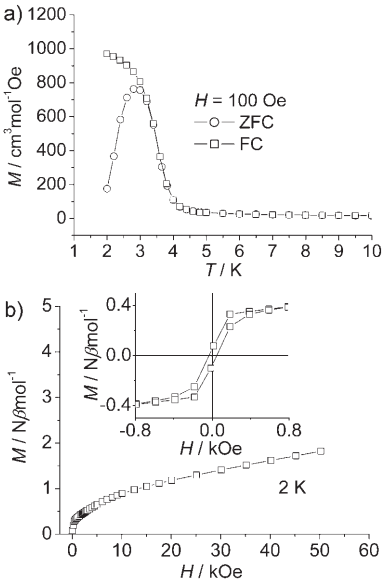

Figure 10. a) Plots of FC and ZFC magnetization for **5**. b) M versus H plot at 2 K for **5**. The inset is the hysteresis loop for **5**.

phase transition at about 2.9 K, where the in-phase part χ_m' reaches a maximum, and no obvious out-of-phase χ_m'' reflection.

Spin ordering of **5** was explored by measuring the ZFC and FC magnetization at 100 Oe (Figure 10a). As expected, both ZFC and FC curves show abrupt increases below 3.8 K and then diverge at about 3.0 K. The magnetization versus field plot at 2 K (Figure 10b) also confirms the observed weak ferromagnetism:[15] at low field, magnetization increases steeply with increasing magnetic field; at higher field, magnetization increases at a slower rate and in an almost linear fashion but finally only reaches about $1.82\,N\beta\,mol^{-1}$ at 50 kOe, far from the expected saturation value of $8.0\,N\beta\,mol^{-1}$ (for two Mn^{III} ions: $g=2$, $S=2$). The small magnetization at high field further proves the state of weak ferromagnetism arising from spin canting in **5**. Furthermore, a small hysteresis loop (inset) at 2 K was detected in the ordered phase with a coercive field of 40 Oe and a remanent magnetization of $0.066\,N\beta\,mol^{-1}$. The temperature dependence of the ac magnetic susceptibilities (see Figure S8 in the Supporting Information) verifies the weak ferromagnetic phase transition at about 3.8 K, where the in-phase part χ_m' reaches a maximum, while the out-of-phase part χ_m'' begins to show nonzero values. By considering ZFC/FC, isothermal magnetization, and ac susceptibility data, we can safely conclude that **5** exhibits weak ferromagnetism originating from spin canting below the critical temperature of $T_C=3.8$ K. The canting angle α is estimated to be about 0.47° from the expression $\sin\alpha = M_R/M_s$.[16]

The low-temperature magnetic properties of **6** are similar to those of **5**. A difference is that the ZFC/FC plots (Figure 11a) measured at 20 Oe first exhibit sharp peaks at about 3.2 K and then diverge at about 2.8 K after abrupt decreases. However, this does not influence the weak ferromagnetic character of **6** caused by spin canting, which is confirmed by measurements of isothermal magnetization at 1.9 K (Figure 11b). The shape of the M versus H curve is very similar to that of **5**, and a small hysteresis loop can be observed with a coercive field of 54 Oe and a remanent magnetization of $0.13\,N\beta\,mol^{-1}$. Moreover, the peak in the in-phase component χ_m' of the ac susceptibility at about 3.2 K (Figure 11c) indicates a magnetic phase transition.[17] The nonzero out-of-phase component χ_m'' supports a ferromagnetic nature of the transition, although it has a frequency dependence affecting mostly the magnitude of the peak and not its position. Therefore, complex **6** is still regarded as a weak ferromagnet due to spin canting below the critical temperature of $T_C=3.2$ K with a canting angle of 0.93°.

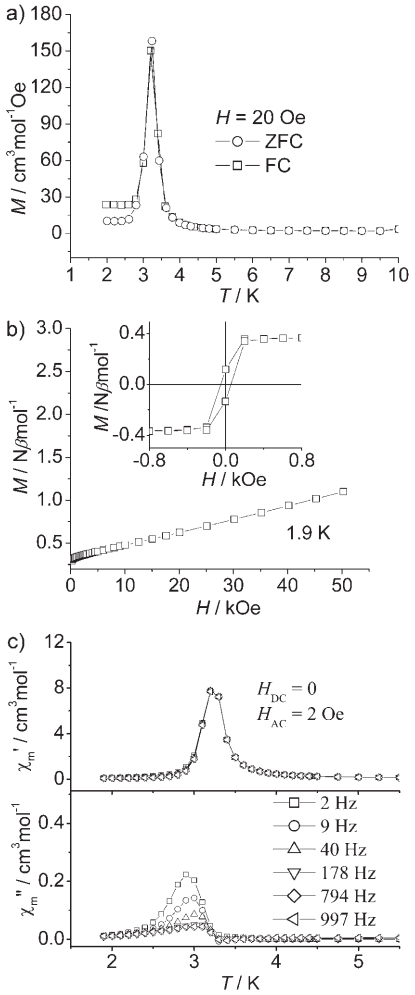

Figure 11. a) Plots of FC and ZFC magnetization for **6**. b) M versus H plot at 1.9 K for **6**. The inset is the hysteresis loop for **6**. c) Temperature dependence of ac susceptibility for **6**.

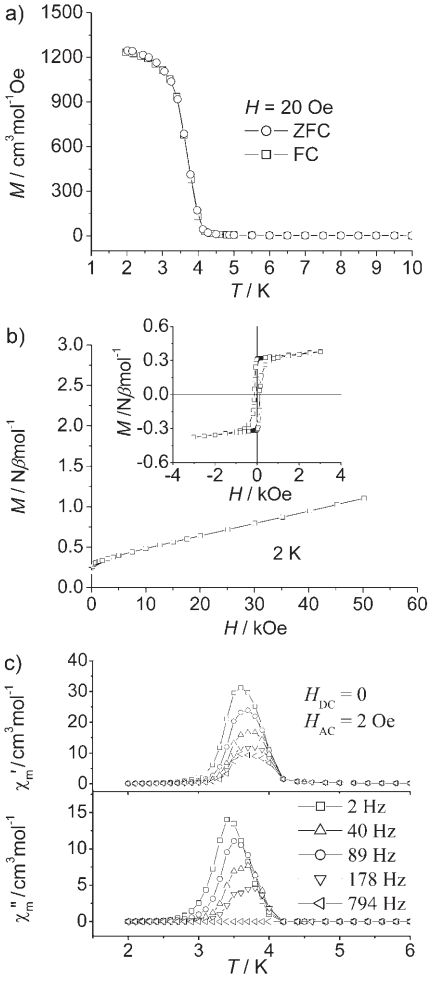

Figure 12. a) Plots of FC and ZFC magnetization for **7**. b) M versus H plot at 1.9 K for **7**. The inset is the hysteresis loop for **7**. c) Temperature dependence of ac susceptibility for **7**.

The magnetic behavior of **7** in the low-temperature region is similar to those of **5** and **6**. The ZFC and FC $M(T)$ data at 20 Oe (Figure 12a) reveal weak ferromagnetism related to spin canting below $T_C = 3.6$ K. The weak ferromagnetism is further supported by the M versus H plot (Figure 12b) measured at 2 K with a similar shape to those of **5** and **6**. Also, the hysteresis loop (inset) observed at 2 K, which is larger than those of **5** and **6**, suggests a weak ferromagnetically ordered phase in **7** with a coercive field of 254 Oe and a remanent magnetization of $0.35\,N\beta\,\mathrm{mol}^{-1}$. The temperature dependence of the ac magnetic susceptibilities (Figure 12c) verifies the occurrence of a weakly ferromagnetic phase at about 3.8 K, where the in-phase part χ_m' exhibits peaks while the out-of-phase part χ_m'' begins to show nonzero values. Interestingly, both χ_m' and χ_m'' components display frequency dependence mainly affecting the magnitude of the peak. However, the peak position of χ_m'' moves slightly to lower temperature with rising frequency, different from that of **5** or **6**.

Further magnetic measurements on **4** and **8** showed that their magnetic behaviors are very similar and only show simple antiferromagnetic coupling without any anomaly in the low-temperature range. In the plots of field dependence of magnetization at 2.0 K for **4** and **8** (see Figure S9 in the Supporting Information), the values increase nearly in line and only reach very small values ($0.72\,N\beta\,\mathrm{mol}^{-1}$ for **4**, and $1.00\,N\beta\,\mathrm{mol}^{-1}$ for **8**) at a high field of 50 kOe, which are far from the expected saturation value of $8.0\,N\beta\,\mathrm{mol}^{-1}$; this again confirms AF interaction.

The magnetic properties of Mn^{III} dimer **9** are similar to those of **4** and **8**, as shown in Figure 13. From the $\chi_m T$ versus T and χ_m^{-1} versus T plots (Figure 13a), the $\chi_m T$ value at room temperature is 5.77 $\mathrm{cm^3\,mol^{-1}\,K}$, in accordance with the theoretical value for two spin-only high-spin Mn^{III} ions. On cooling, values of $\chi_m T$ that keep decreasing in the 300–1.9 K range indicate overall antiferromagnetic coupling in **9**. The magnetic susceptibility above 50 K can be well fit to the Curie–Weiss law with $C = 6.09\ \mathrm{cm^3\,mol^{-1}\,K}$ and $\theta = -17.0$ K. The Curie constant C is also close to the expected value of

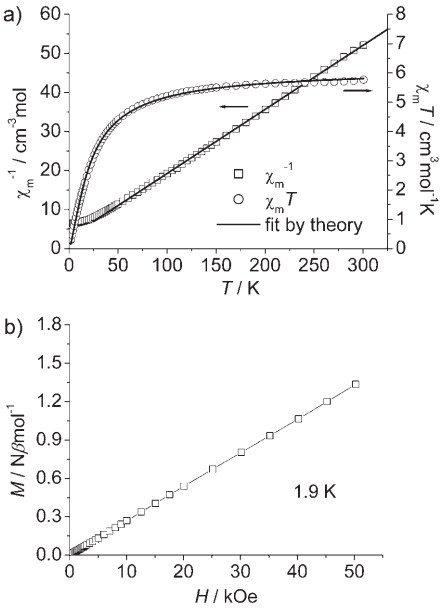

Figure 13. a) χ_m and χ_m^{-1} versus T plots in an applied field of 1 kOe with a theoretical fit for **9**. b) M versus H plot at 1.9 K for **9**.

6.0 $cm^3 mol^{-1} K$ for two noninteracting Mn^{III} ions ($S=2$, $g=2$), and the negative θ value further confirms the presence of antiferromagnetic interaction in **9**. The M versus H plot measured at 1.9 K (Figure 13b) shows that the magnetization increases almost linearly from 0 to 50 kOe and reaches 1.34 $N\beta mol^{-1}$, far from the theoretic saturation value 8.0 $N\beta mol^{-1}$ for two spin-only Mn^{III} ions, which again confirms antiferromagnetic interaction between Mn^{III} ions.

Estimation of coupling constants and discussion: Considering that transmission of magnetic coupling through the three-atom NCNH bridge is possibly much weaker than that through the single-atom phenolate oxygen bridge, we used the dinuclear Mn^{III}_2 model to fit the magnetic susceptibility data of complexes **3**–**9**.[18] The total spin Hamiltonian taking into account the Zeeman perturbation for the dimer is given by Equation (1), where J is the Mn–Mn exchange parameter through phenolate oxygen atom and S_{Mn} and g_{Mn} are spin and the local g tensor associated with Mn^{III}. The interdimer interaction, that is, the Mn–Mn exchange parameter through the NCNH bridge, was considered in the mean-field approximation and appears as zJ' in the expression of $\chi_m T$ used to analyze the experimental data [Eq. (2)].

$$\mathrm{H} = -2J\hat{S}_{\mathrm{Mn1}}\hat{S}_{\mathrm{Mn2}} + g_{\mathrm{Mn}}\beta(\hat{S}_{\mathrm{Mn1}} + \hat{S}_{\mathrm{Mn2}})H \quad (1)$$

$$\chi_{\mathrm{M}}T = \frac{Ng^2\beta^2F(J,T)T}{kT - zJ'F(J,T)} \quad (2)$$

where [Eq. (3)]

$$F(J,T) = \frac{60 + 2\exp(-18J/kT) + 10\exp(-14J/kT) + 28\exp(-8J/kT)}{9 + 3\exp(-18J/kT) + 5\exp(-14J/kT) + 7\exp(-8J/kT) + \exp(-20J/kT)}$$

From the best-fitting results (Table 5), the Mn–Mn exchange parameter through the phenolate oxygen atom is in the range of -1.8 to $-3.4\ cm^{-1}$, close to those for Mn^{III}_2

Table 5. Best-fitting results for the Mn^{III}_2 model of **3**–**9**.

	g	J [cm^{-1}]	zJ' [cm^{-1}] ($z=2$)	R
3 (10–300 K)	2.031	−2.7	−0.87	1.5×10^{-4}
4 (2–300 K)	2.025	−3.4	−0.94	1.6×10^{-4}
5 (20–300 K)	2.014	−2.2	−0.67	4.3×10^{-5}
6 (6–300 K)	2.044	−3.2	−0.79	5.4×10^{-4}
7 (10–300 K)	2.014	−2.8	−1.10	1.4×10^{-4}
8 (6–300 K)	2.029	−2.9	−1.20	2.9×10^{-4}
9 (2–300 K)	2.025	−1.8	−0.64	1.3×10^{-4}

complexes bridged by a phenolate oxygen atom reported in the literature,[19] while the magnetic coupling constant between Mn^{III} ions linked by the $NCNH^-$ ligand is much smaller, in the range of -0.32 to $-0.60\ cm^{-1}$, in agreement with the magnitude of the type I complexes. In addition, the fact that both of these values are negative confirms dominant antiferromagnetic interaction between Mn^{III} ions in these complexes, especially for the new type of three-atom bridge $NCNH^-$, which transmits antiferromagnetic coupling, comparable to the familiar N_3^- ligand. However, the magnitude of the exchange interaction in these NCNH-bridged complexes is much smaller than that of the azide-bridged Mn^{III} salen complex $[Mn(salen)N_3]$.[12b]

Similar to the azide-bridged linear chain,[12b] the hydrogencyanamide-bridged one-dimensional polymers with long axial bonds presented here should have only one dominant exchange pathway due to the small axial overlap, and this results in a weak antiferromagnetic interaction. The only magnetic orbital is that derived from the Mn^{III} d_{z^2} orbital, which may make a significant contribution to the coupling. The axial ligands will mainly provide a σ-type superexchange pathway, while a mechanism involving the π orbitals of the bridging group is conceivable. The weak ferromagnetism in these NCNH-bridged Mn^{III} complexes arises from spin canting of the antiferromagnetically interacting Mn^{III} ions, and the origin of the spin canting should be mainly the asymmetric interaction between the neighboring Mn^{III} ions, in combination with possible local anisotropy of Mn^{III} ions.[15c]

Conclusion

Nine hydrogencyanamide-bridged Mn^{III} coordination complexes with a series of tetradentate Schiff base ligands were structurally and magnetically characterized. Their structures can be divided into three types: mononuclear-Mn^{III}-based chains **1** and **2**, Mn^{III}-dimer-based chains **3**–**8**, and Mn^{III} dimer **9**, which are all linked through hydrogen bonds into

2D networks. In complexes **3**–**8** with similar structures, the small structural differences mainly depend on the different Schiff base ligands and solvents used in their initial syntheses; complexes **3**/**4** and **5**/**6** are two pairs of similar structures except for the different solvent molecules in the crystal. The different solvent molecules in the crystal structures cause changes in the Mn-N-C angles (Table 4): for complexes **3**, **5**, and **7** with methanol molecules, the difference between the two Mn-N-C angles is about 4°, whereas for complexes **4**, **6**, and **8** with ethanol molecules, the difference is only about 1°. Complexes **1**–**9** all exhibit overall AF coupling between Mn^{III} ions, which indicates that the $\mu_{1,3}$-NCNH bridge mostly transmits antiferromagnetic coupling, like the widely investigated $\mu_{1,3}$-N_3 bridge. However, because of the effects of different Schiff base ligands L and/or solvent molecules S in **1**–**9**, their magnetic properties differ at low temperatures: 1) mononuclear-Mn^{III}-based complexes **1** and **2** both show field-dependent weak ferromagnetic ordering due to spin canting, along with AF spin reorientation; 2) complex **3** exhibits a metamagnetic behavior; 3) complexes **5**–**7** also show weak ferromagnetism at low temperature due to spin canting; 4) complexes **4**, **8**, and **9** do not show any special magnetic phase transition down to 1.9 K but an AF interaction. All in all, the $\mu_{1,3}$-NCNH bridge favors the occurrence of weak ferromagnetism due to spin canting in view of its asymmetrical resonance structure in these chains. Moreover, the complexes with ethanol molecules seem to lose the weak ferromagnetism compared with the complexes with methanol molecules. Although the magnetic interaction mediated by hydrogencyanamide in complexes **1**–**9** is weaker than that mediated by the azide bridge, this work provides an unprecedented series of one-dimensional models for studying the coordination chemistry and magnetic properties of cyanamide complexes, and further enriches the field of molecule-based magnetic materials.

Experimental Section

General procedure: All starting materials were commercially available, reagent-grade, and used as purchased without further purification. The tetradentate Schiff base ligands H_2L were synthesized by mixing the corresponding salicylaldehyde and 1,2-diaminoethane in a 2:1 molar ratio in ethanol according to the literature.[20]

Caution! *Perchlorate salts of metal complexes with organic ligands are potentially explosive. Only small quantities of these complexes should be prepared and handled with proper protection.*

$[Mn^{III}(5\text{-Brsalen})(\mu_{1,3}\text{-NCNH})]_n$ (1): Complex **1** was prepared by adding a methanolic solution (10 mL) of $NCNH_2$ (0.011 mg, 0.25 mmol) to a methanol solution (20 mL) of $Mn(ClO_4)_2{\cdot}6H_2O$ (0.090 mg, 0.25 mmol), $H_2$5-Brsalen (0.107 mg, 0.25 mmol), and NaOH (0.02 mg, 0.50 mmol) with stirring at room temperature for about 24 h. Small, deep red crystals were obtained in 40% yield by suction filtration, washed with methanol, and dried in air. IR (KBr): $\tilde{\nu}$ = 654(m), 688(m), 800(w), 818(w), 1176(w), 1297(s), 1375(m), 1452(m), 1525(m), 1593(w), 1630(s), 2096(s), 2929(w), 2968(w), 3297(w) cm^{-1}; elemental analysis (%) calcd for $C_{17}H_{13}Br_2MnN_4O_2$: C 39.26, H 2.52, N 10.77; found: C 39.02, H 2.50, N 10.68.

$[Mn^{III}(5\text{-Clsalen})(\mu_{1,3}\text{-NCNH})]_n$ (2): The preparation of **2** was analogous to that of **1** but we replaced $Mn(ClO_4)_2{\cdot}6H_2O$ and $H_2$5-Brsalen with $(CH_3COO)_2{\cdot}4H_2O$ and $H_2$5-Clsalen, respectively. IR (KBr): $\tilde{\nu}$ = 707(m), 799(m), 969(w), 1040(w), 1178(m), 1289(s), 1299(s), 1373(m), 1455(m), 1527(m), 1597(m), 1638(s), 2142(s), 2927(w), 2959(w), 3058(w), 3356(w) cm^{-1}; elemental analysis (%) calcd for $C_{17}H_{13}Cl_2MnN_4O_2$: C 47.36, H 3.04, N 12.99; found: C 47.22, H 2.98, N 13.10.

$[Mn^{III}_2(salen)_2(\mu_{1,3}\text{-NCNH})]ClO_4{\cdot}CH_3OH$ (3): A similar preparation to that presented for **1** was used for **3** but with H_2salen instead of $H_2$5-Brsalen. Dark brown crystals were collected by suction filtration, washed with methanol, and dried in air (yield: 80%). IR (KBr): $\tilde{\nu}$ = 757(m), 801(m), 904(m), 1090(s), 1295(m), 1445(m), 1542(m), 1600(s), 1622(s), 2107(s), 2148(m), 2927(w), 3029(w), 3062(w), 3334(w), 3600(w) cm^{-1}; elemental analysis (%) calcd for $C_{34}H_{33}ClMn_2N_6O_9$: C 50.11, H 4.08, N 10.31; found: C 49.80, H 4.07, N 10.35.

$[Mn^{III}_2(salen)_2(\mu_{1,3}\text{-NCNH})]ClO_4{\cdot}C_2H_5OH$ (4): $Mn(ClO_4)_2{\cdot}6H_2O$ (0.090 g, 0.25 mmol) was added to an ethanol solution (20 mL) of H_2salen (0.082 g, 0.25 mmol) and triethylamine (0.070 mL, 0.50 mmol). After the brown solution was stirred for 4 h, an ethanol solution (10 mL) of H_2NCN (0.0105 g, 0.25 mmol) was slowly added, and stirring was continued at room temperature for about 24 h. Dark brown crystals were collected by suction filtration, washed with ethanol, and dried in air (yield: 80%). IR (KBr): $\tilde{\nu}$ = 757(m), 801(m), 905(m), 1093(s), 1296(m), 1445(m), 1542(m), 1601(s), 1624(s), 2115(s), 2145(m), 2927(w), 2968(w), 3066(w), 3348(w), 3550(w) cm^{-1}; elemental analysis (%) calcd for $C_{35}H_{35}ClMn_2N_6O_9$: C 50.71, H 4.26, N 10.14; found: C 50.79, H 4.21, N 10.20.

$[Mn^{III}_2(5\text{-Fsalen})_2(\mu_{1,3}\text{-NCNH})]ClO_4{\cdot}CH_3OH$ (5): Following the same procedure as for preparation of **4**, H_2salen was replaced by $H_2$5-Fsalen, and the ethanol solvent by methanol (yield: 82%). IR (KBr): $\tilde{\nu}$ = 781(m), 809(m), 1090(m), 1286(m), 1463(s), 1548(s), 1628(s), 2109(m), 2148(m), 2937(w), 3063(w), 3359(w), 3530(w) cm^{-1}; elemental analysis (%) calcd for $C_{34}H_{29}ClF_4Mn_2N_6O_9$: C 46.04, H 3.30, N 9.48; found: C 45.56, H 3.20, N 9.25.

$[Mn^{III}_2(5\text{-Fsalen})_2(\mu_{1,3}\text{-NCNH})]ClO_4{\cdot}C_2H_5OH$ (6): Following the same procedure as for preparation **4**, H_2salen was replaced by $H_2$5F-salen (yield: 78%). IR (KBr): $\tilde{\nu}$ = 783(m), 806(m), 1091(s), 1289(m), 1464(s), 1550(s), 1629(s), 2113(s), 2144(w), 2889(w), 2933(w), 3071(w), 3352(w), 3540(w) cm^{-1}; elemental analysis (%) calcd for $C_{35}H_{31}ClF_4Mn_2N_6O_9$: C 46.66, H 3.47, N 9.33; found: C 46.45, H 3.60, N 9.33.

$[Mn^{III}_2(5\text{-Clsalen})_2(\mu_{1,3}\text{-NCNH})]ClO_4{\cdot}CH_3OH$ (7): Following the same procedure as for preparation of **1**, $H_2$5-Brsalen was replaced by $H_2$5-Clsalen (yield: 60%). IR (KBr): $\tilde{\nu}$ = 711(m), 847(m), 1092(s), 1290(m), 1456(m), 1532(m), 1627(s), 2109(s), 2936(w), 3085(w), 3341(w), 3556(w) cm^{-1}; elemental analysis (%) calcd for $C_{34}H_{29}Cl_5Mn_2N_6O_9$: C 42.86, H 3.07, N 8.82; found: C 42.78, H 3.01, N 8.75.

$[Mn^{III}_2(5\text{-}OCH_3\text{salen})_2(\mu_{1,3}\text{-NCNH})]ClO_4{\cdot}C_2H_5OH$ (8): $Mn(ClO_4)_2{\cdot}6H_2O$ (0.054 g, 0.15 mmol) was added to an ethanol solution (20 mL) of $H_2$5-OCH_3salen (0.049 g, 0.15 mmol) and triethylamine (0.042 mL, 0.30 mmol). After the brown solution was stirred for 4 h, a methanol solution (10 mL) of H_2NCN (0.0063 g, 0.15 mmol) was slowly added, and stirring was continued at room temperature for about 24 h. Dark brown crystals were collected by suction filtration, washed with methanol, and dried in air (yield: 85%). IR (KBr): $\tilde{\nu}$ = 775(m), 807(m), 972(w), 1092(s), 1285(s), 1468(s), 1545(s), 1612(s), 1621(s), 2112(s), 2937(w), 3075(w), 3340(w), 3595(w) cm^{-1}; elemental analysis (%) calcd for $C_{39}H_{43}ClMn_2N_6O_{13}$: C 49.35, H 4.57, N 8.85; found: C 49.29, H 4.54, N 8.76.

$\{[Mn^{III}(3\text{-}OCH_3\text{salen})(H_2O)]_2(\mu_{1,3}\text{-NCNH})\}ClO_4{\cdot}0.5H_2O$ (9): Following the same procedure as for preparation of **8**, $H_2$5-OCH_3salen was replaced by $H_2$3-OCH_3salen, and the ethanol solvent by methanol (yield: 75%). IR (KBr): $\tilde{\nu}$ = 737(m), 860(m), 1085(s), 1222(m), 1253(s), 1298(m), 1444(m), 1471(m), 1602(m), 1626(s), 2128(m), 2840(w), 2938(w), 3062(w), 3427(m), 3600(w) cm^{-1}; elemental analysis (%) calcd for $C_{37}H_{42}ClMn_2N_6O_{14.5}$: C 46.88, H 4.47, N 8.87; found: C 46.26, H 4.42, N 8.62.

Physical measurements: Elemental analyses of carbon, hydrogen, and nitrogen were carried out with an Elementar Vario EL. Microinfrared spec-

troscopy studies were performed on a Magna-IR 750 spectrophotometer in the 4000–500 cm^{-1} region.

Magnetic measurements: Variable-temperature magnetic susceptibility, zero-field ac magnetic susceptibility, and field dependence of magnetization were measured on an Oxford Maglab 2000 System or Quantum Design MPMSXL7 (SQUID) magnetometer. The experimental susceptibilities were corrected for the diamagnetism of the constituent atoms (Pascal's tables).

X-ray crystallography: The data of all complexes were collected on a Nonius Kappa-CCD with $Mo_{K\alpha}$ radiation ($\lambda = 0.71073$ Å) at 293 K. The structures were solved by direct methods and refined by the full-matrix least-squares technique on F^2 using the SHELXL97 program. All non-hydrogen atoms were refined anisotropically. Hydrogen atoms defined by the stereochemistry were placed at their calculated positions and allowed to ride on their host carbon atoms. Crystallographic data are listed in Table 1, and selected bond lengths and angles in Table 2.

CCDC-234944 (**1**), CCDC-272460 (**2**), CCDC-240678 (**3**), CCDC-272458 (**4**), CCDC-297408 (**5**), CCDC-297407 (**6**), CCDC-272459 (**7**), CCDC-272457 (**8**), and CCDC-297409 (**9**) contain the supplementary crystallographic data for this paper. These data can be obtained free of charge from the Cambridge Crystallographic Data Centre via www.ccdc.cam.ac.uk/data_request/cif.

Acknowledgements

This work is supported by NSFC (20221101, 20490210), and the National Basic Research Program of China (2006CB601102).

[1] a) S. Ferlay, T. Mallah, R. Ouahes, P. Veillet, M. Verdaguer, *Nature* **1995**, *378*, 701–703; b) O. Sato, T. Iyoda, A. Fujishima, K. Hashimoto, *Science* **1996**, *272*, 704–705; c) H. Tamaki, Z. J. Zhong, N. Matsumoto, S. Kida, K. Koikawa, N. Achiwa, H. Okawa, *J. Am. Chem. Soc.* **1992**, *114*, 6974–6979; d) J. Ribas, A. Escuer, M. Monfort, R. Vicente, R. Cortes, L. Lezama, T. Rojo, *Coord. Chem. Rev.* **1999**, *193*, 1027–1068, and references therein; e) B. Q. Ma, S. Gao, G. Su, G. X. Xu, *Angew. Chem.* **2001**, *113*, 448–451; *Angew. Chem. Int. Ed.* **2001**, *40*, 434–437; f) J. Larionova, J. Sanchiz, S. Gohlen, L. Ouahab, O. Kahn, *Chem. Commun.* **1998**, 953–954.

[2] a) M. Becker, M. Jansen, A. Lieb, W. Milius, W. Schnick, *Z. Anorg. Allg. Chem.* **1998**, *624*, 113–118; b) M. Becker, J. Nuss, M. Jansen, *Z. Anorg. Allg. Chem.* **2000**, *626*, 2505–2508.

[3] U. Berger, W. Schnick, *J. Alloys Compd.* **1994**, *206*, 179–184.

[4] a) R. Srinivasan, M. Ströbele, H. J. Meyer, *Inorg. Chem.* **2003**, *42*, 3406–3411; b) C. H. Hu, R. K. Kremer, R. Dronskowski, *Inorg. Chem.* **2004**, *43*, 5884–5890; c) W. P. Liao, R. Dronskowski, *Inorg. Chem.* **2006**, *45*, 3828–3830.

[5] X. H. Liu, M. Krott, P. Müller, C. H. Hu, H. Lueken, R. Dronskowski, *Inorg. Chem.* **2005**, *44*, 3001–3003.

[6] a) M. Becker, M. Jansen, *Z. Anorg. Allg. Chem.* **2000**, *626*, 1639–1641; b) X. H. Liu, P. Müller, P. Kroll, R. Dronskowski, *Inorg. Chem.* **2002**, *41*, 4259–4265; c) X. H. Liu, P. Kroll, R. Dronskowski, *Z. Anorg. Allg. Chem.* **2001**, *627*, 1682–1686; d) M. H. V. Huynh, P. S. White, C. A. Carter, T. J. Meyer, *Angew. Chem.* **2001**, *113*, 3027–3029; *Angew. Chem. Int. Ed.* **2001**, *40*, 3037–3039; e) R. Cao, K. Tatsumi, *Chem. Commun.* **2002**, 2144–2145.

[7] a) F. Meyer, I. Hyla-Krypsin, E. Kaifer, P. Kircher, *Eur. J. Inorg. Chem.* **2000**, *39*, 771–781; b) P. Chaudhuri, K. Wieghardt, B. Nuber, J. Weiss, *J. Chem. Soc. Chem. Commun.* **1985**, 265–266; c) Y. Tanabe, S. Kuwata, Y. Ishii, *J. Am. Chem. Soc.* **2002**, *124*, 6528–6529.

[8] S. R. Batten, K. S. Murray, *Coord. Chem. Rev.* **2003**, *246*, 103–130.

[9] M. Yuan, S. Gao, H. L. Sun, G. Su, *Inorg. Chem.* **2004**, *43*, 8221–8223.

[10] a) F. J. Zhang, A. H. Ding, *Fine and Specialty Chemicals* (in Chinese) **2002**, *10*, 17–18; b) R. J. Lewis, Sr. , *Hazardous Chemicals Desk Reference*, 3rd ed., Van Nostrand Reinhold, New York, **1993**, p. 359.

[11] a) M. L. Brader, E. W. Ainscough, E. N. Baker, A. M. Brodie, S. L. Ingham, *J. Chem. Soc. Dalton Trans.* **1990**, 2785–2792; b) E. W. Ainscough, E. N. Baker, M. L. Brader, A. M. Brodie, S. L. Ingham, J. M. Waters, J. V. Hanna, P. C. Healy, *J. Chem. Soc. Dalton Trans.* **1991**, 1243–1249; c) S. M. P. R. M. Cunha, M. F. C. Guedes da Siva, A. J. L. Pombeiro, *J. Chem. Soc. Dalton Trans.* **2002**, 1791–1799.

[12] a) B. J. Kennedy, K. S. Murray, *Inorg. Chem.* **1985**, *24*, 1552–1557; b) A. Panja, N. Shaikh, P. Vojtišek, S. Gao, P. Banerjee, *New J. Chem.* **2002**, *26*, 1025–1028; c) K. R. Reddy, M. V. Rajasekharan, J. P. Tuchagues, *Inorg. Chem.* **1998**, *37*, 5978–5982.

[13] G. R. Wagner, S. A. Friendberg, *Phys. Lett.* **1964**, *9*, 11–13.

[14] a) C. Y. Weng, Ph.D. Thesis, Carnegie Institute of Technology, USA, **1968**; b) W. Hiller, J. Strahle, A. Datz, M. Hanack, W. E. Hatfield, L. W. ter Haar, P. Guetlich, *J. Am. Chem. Soc.* **1984**, *106*, 329–335.

[15] a) R. L. Carlin, A. J. Van Duyneveldt, *Magnetic Properties of Transition Metal Complexes, Vol. 2*, Springer, New York, **1977**, p. 184; b) E. Bakalbassis, P. Bergerat, O. Kahn, S. Jeannin, Y. Jeannin, Y. Dromzee, M. Guillot, *Inorg. Chem.* **1992**, *31*, 625–631; c) S. Sailaja, K. R. Reddy, M. V. Rajasekharan, C. Hureau, E. Rivière, J. Cano, J.-J. Girerd, *Inorg. Chem.* **2003**, *42*, 180–186.

[16] O. Kahn, *Molecular Magnetism*; VCH, New York, **1993**.

[17] J. A. Mydosh, *Spin Glasses, An Experimental Introduction*, Taylor and Francis, London, **1993**, p. 64.

[18] a) O. Kahn, *Struct. Bonding (Berlin)* **1987**, *68*, 89; b) R. Karmakar, C. R. Choudhury, G. Bravic, J. P. Sutter, S. Mitra, *Polyhedron* **2004**, *23*, 949–954.

[19] a) N. Matsumoto, Z. Zhong, H. Okawa, S. Kida, *Inorg. Chim. Acta* **1989**, *160*, 153–157; b) J. A. Bonadies, M. L. Kirk, M. S. Lah, D. P. Kessissoglou, W. E. Hatfield, V. L. Pecoraro, *Inorg. Chem.* **1989**, *28*, 2037–2044.

[20] a) N. Aurangzeb, C. E. Hulme, C. A. McAuliffe, R. G. Pritchard, M. Watkinson, A. Garcia-Deibe, M. R. Bermejo, A. Sousa, *J. Chem. Soc. Chem. Commun.* **1992**, 1524–1525; b) N. Aurangzeb, C. E. Hulme, C. A. McAuliffe, R. G. Pritchard, M. Watkinson, M. R. Bermejo, A. Sousa, *J. Chem. Soc. Chem. Commun.* **1994**, 2193–2194.

Received: August 13, 2006
Published online: December 15, 2006

